Annual Review of Materials Research

Circular Steel for Fast Decarbonization: Thermodynamics, Kinetics, and Microstructure Behind Upcycling Scrap into High-Performance Sheet Steel

Dierk Raabe,[1] Matic Jovičević-Klug,[1] Dirk Ponge,[1] Alexander Gramlich,[2] Alisson Kwiatkowski da Silva,[1] A. Nicholas Grundy,[3] Hauke Springer,[1,2] Isnaldi Souza Filho,[1,4] and Yan Ma[1]

[1]Max Planck Institute for Sustainable Materials, Düsseldorf, Germany; email: d.raabe@mpie.de, y.ma@mpie.de

[2]Steel Institute, RWTH Aachen University, Aachen, Germany

[3]Thermo-Calc Software AB, Solna, Sweden

[4]Institut Jean Lamour, CNRS (UMR 7198), Université de Lorraine, Nancy, France

Annu. Rev. Mater. Res. 2024. 54:247–97

First published as a Review in Advance on April 29, 2024

The *Annual Review of Materials Research* is online at matsci.annualreviews.org

https://doi.org/10.1146/annurev-matsci-080222-123648

Keywords

recycling, green steel, scrap, sustainability, metallurgy, decarbonization, microstructure

Abstract

Steel production accounts for approximately 8% of all global CO_2 emissions, with the primary steelmaking route using iron ores contributing approximately 80% of those emissions, mainly due to the use of fossil-based reductants and fuel. Hydrogen-based reduction of iron oxide is an alternative for primary synthesis. However, to counteract global warming, decarbonization of the steel sector must proceed much faster than the ongoing transition kinetics in primary steelmaking. Insufficient supply of green hydrogen is a particular bottleneck. Realizing a higher fraction of secondary steelmaking is thus gaining momentum as a sustainable alternative to primary production.

Steel production from scrap is well established for long products (rails, bars, wire), but there are two main challenges. First, there is not sufficient scrap available to satisfy market needs. Today, only one-third of global steel demand can be met by secondary metallurgy using scrap since many steel products have a lifetime of several decades. However, scrap availability will increase to about two-thirds of total demand by 2050 such that this sector will grow massively in the next decades. Second, scrap is often too contaminated to produce high-performance sheet steels. This is a serious obstacle because advanced products demand explicit low-tolerance specifications for safety-critical and high-strength steels, such as for electric vehicles, energy conversion and grids, high-speed trains, sustainable buildings, and infrastructure. Therefore, we review the metallurgical and microstructural challenges and opportunities for producing high-performance sheet steels via secondary synthesis. Focus is placed on the thermodynamic, kinetic, chemical, and microstructural fundamentals as well as the effects of scrap-related impurities on steel properties.

1. DISRUPTIVE ENHANCEMENT OF STEEL SUSTAINABILITY THROUGH RECYCLING

The steel sector causes approximately 30% of all global industrial CO_2 emissions in producing 1.9 billion tonnes of steel per year (1–5). On a global average, current production technologies release nearly 2 t of CO_2 per tonne of steel produced. The majority comes from blast furnaces (delivering a near-eutectic Fe–C alloy called pig iron) and oxygen converters (producing steel from pig iron), a coupled route that accounts for approximately 80% of global steel production (2). Therefore, other primary synthesis methods are being investigated to mitigate CO_2 emissions in this sector. A process with a high technology readiness level is direct reduction in shaft reactors. In this approach, centimeter-sized polycrystalline sintered oxide pellets are exposed to a reducing gas (today, mostly H_2 plus CO syngas mixtures made from methane), producing 93–98% metalized sponge iron. This technology is in operation worldwide but accounts for a small fraction, approximately 6–7%, of global steel production (2). Replacing the currently used fossil reductants with green hydrogen in direct reduction reactors is one of the most promising sustainable pathways, capable of at least partially replacing blast furnace production (6–10). This approach could potentially drastically reduce CO_2 emissions in the steel sector, provided the hydrogen comes from sustainable sources (7, 11–13). Other green steel production methods under development, but not yet at the same technology readiness level, are hydrogen plasma-based smelting reduction methods (12, 14), ammonia-based direct reduction (11), and cathodic deposition of iron from fused-salt electrolysis of iron oxide (15, 16).

A problem that all these alternative technologies share is the long transition time required to realize their expected CO_2 mitigation, probably up to 1–3 decades on a global scale (17–20). This has several reasons. The necessary research, as well as the construction of industrial plants, will take several decades on a scale as massive as global steel production (4, 21, 22). The transition from the blast furnace–basic oxygen converter (BF–BOF) route to hydrogen-based direct reduction (which is the likely future workhorse technology) will require intensive research, tens of billions of euros of investments, and time to build and optimize these new facilities. Furthermore, at least 250–300 million t of sustainably produced hydrogen will be required per year, an amount that is unlikely to be available in the next few years due to insufficient electrolysis capacity and renewable energy (22–24). The currently available, sustainably produced amount of hydrogen available is three-to-four orders of magnitude below the demand from the steel sector alone (3).

However, decarbonization of the steel industry is an urgent task because reducing emissions over the next two decades is particularly critical to stabilize the climate (**Figure 1**; see also

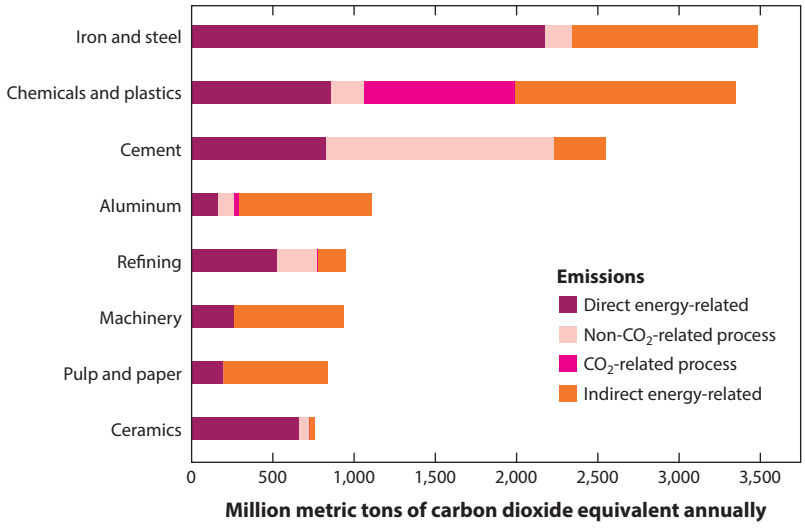

Figure 1

CO_2 emissions caused by steel production compared with other materials. Figure adapted from Reference 22 (CC BY 4.0).

Supplemental Figure 1). This means that CO_2 emissions from the steel sector must be reduced as soon as possible, not 20 or 30 years from now, because CO_2 remains in the atmosphere for centuries once released. Therefore, increasing the utilization of scrap steel for secondary synthesis, that is, recycling, is the fastest and most disruptive way to at least partially decarbonize the steel sector in the coming years (1, 3, 25, 26). With a current fraction of about 28% of global steel production, scrap melting is a long-established standard recycling method and is expected to grow rapidly in the next few years if (*a*) enough electric arc furnaces (EAFs) are installed, (*b*) the energy used to run them increasingly comes from sustainable power generation, and (*c*) the scrap market grows accordingly (27–34). All three criteria are in principle within reach such that secondary synthesis has a realistic chance of providing a rapid route to decarbonizing up to a 30% share of the steel sector, with the potential to grow up to 60–70% by 2040 (35–37).

Supplemental Material >

Recycling through melting scrap in EAFs has the main advantage of directly using electricity, which should ideally come from renewable sources, for heat generation (26, 34, 38, 39). This fact alone reduces the high energy losses associated with heating air, as in conventional furnaces. According to estimates by the World Steel Association, recycling 1 t of steel scrap saves around 1.4–1.5 t of iron ore, 0.5–0.6 t of coal, and 40–75% of the energy required for primary steel production (2, 40). With 1 kg of steel produced from steel scrap instead of through the BF–BOF route, this translates to end-of-life savings of approximately 1.5 kg of CO_2 emissions, 13.4 MJ of primary energy, and 1.4 kg of iron ore, corresponding to reductions of 73%, 64%, and 90%, respectively (**Figure 2**) (31). This means that the potential reduction in CO_2 emissions is enormous when turning from primary to secondary synthesis: Using 1 t of scrap in steel production instead of pig iron from the blast furnace can reduce CO_2 emissions by around 58–64% (17, 28, 29, 41). The exact reduction depends on factors such as the scrap composition, production process, EAF electrodes (inert or graphite), and energy sources used. The last point is particularly important: In the production of steel from scrap via the EAF route, the CO_2 footprint of the supplied energy plays a crucial role. This means that CO_2 reduction via the EAF route depends on the CO_2 footprint of the used electrical energy. The International Energy Agency predicts a CO_2 factor for the

grid in Europe of 80 g/kWh by 2050, which can lead to a CO_2 reduction of 289 kg/t of crude steel for this route or a decrease of 57% in 2050 compared with 1990 (42, 43). If the supplied energy is provided by CO_2-neutral fuels or CO_2-free electrical energy, CO_2 emissions can even be reduced by up to 60 kg/t of crude steel, which is still unavoidably generated by the consumption of graphite electrodes and the use of additives and alloying elements. This corresponds to a CO_2 reduction of 91% for the scrap-based EAF route compared with 1990.

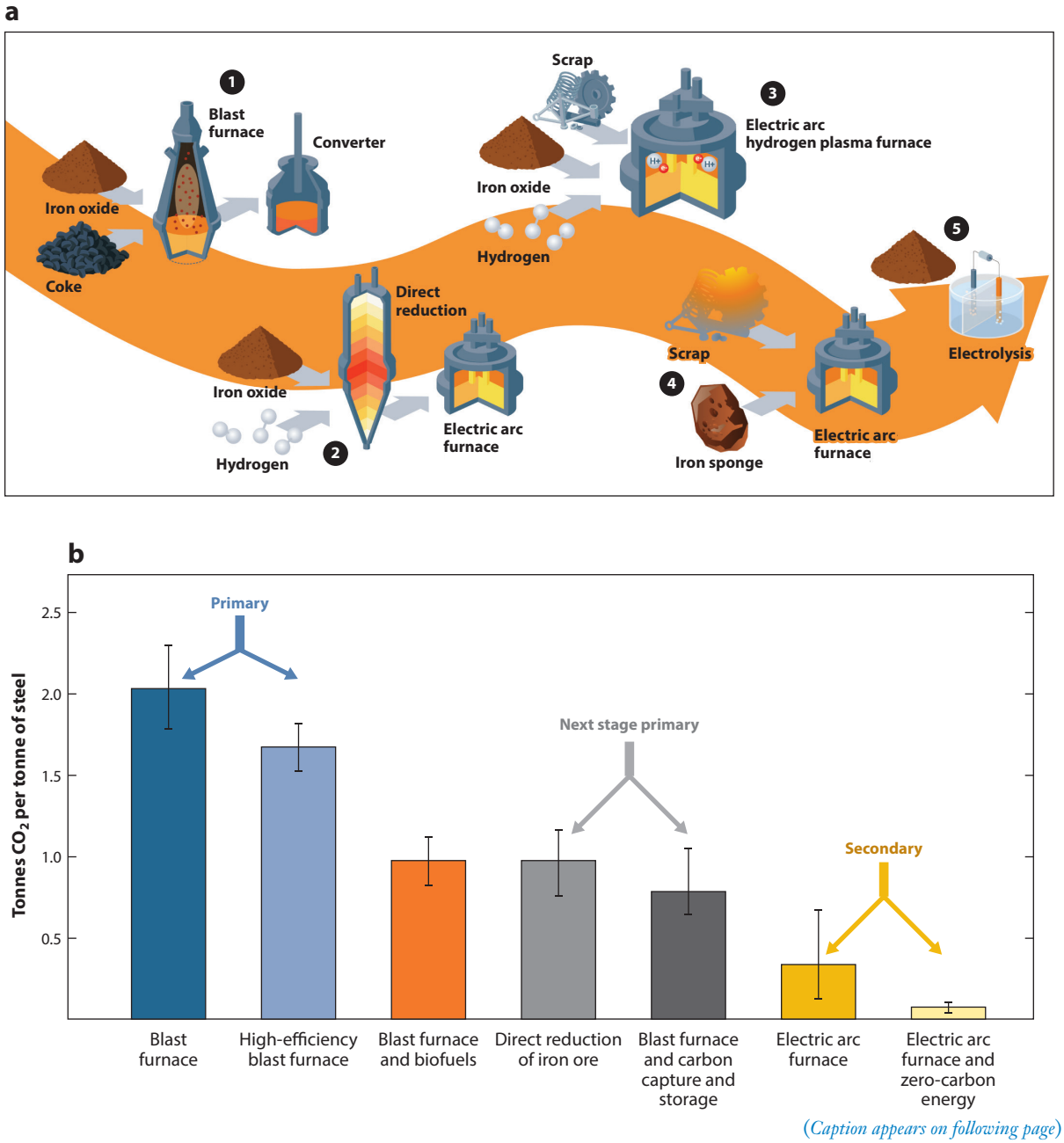

(*Caption appears on following page*)

Figure 2 (*Figure appears on preceding page*)

(*a*) Some of the scalable technologies for the decarbonization of the steel sector: (①) conventional blast furnace and oxygen converter route, 1.8–2.2 t CO_2 per tonne of steel produced; (②) hydrogen-based direct reduction in static shaft reactors, 0.7–1.2 t CO_2 per tonne of steel produced, depending on the origin of the reductant and of the fuel used for heating (these numbers apply to the use of natural gas–based reductant in direct reduction, while even lower numbers of approximately 0.02–0.2 t CO_2 per tonne of steel are claimed when sustainably produced hydrogen and renewable grid electricity are used); (③) hydrogen-based plasma smelting reduction, 0.2–0.8 t CO_2 per tonne of steel produced; (④) secondary synthesis via melting of scrap, 0.1–0.2 t CO_2 per tonne of steel produced; and (⑤) electrolysis based on molten salt–iron oxide mixtures, ionic liquids, or low-temperature alkaline solutions. In all cases substantial variations in these estimates come from the origin and carbon footprint of the reductants, (co-)fueling agents and electrical energy used to heat and operate the electric arc furnaces, etc. (*b*) CO_2 emissions associated with different steelmaking processes with a fairly high technology readiness level for rapid implementation. Note that the real carbon footprint can in all cases be higher when hydrogen is not made from renewables and when fossil electricity is used. Also consider that reduction with hydrogen is an endothermic, not exothermic, reaction such that corresponding aggregates require additional co-fueling and heating. Details about the numbers and underlying technologies can be found in Reference 3.

The success parameters associated with metal recycling are characterized by two main numbers, the end-of-life recycling rate and the recycled fraction used in new alloys. End-of-life recycling rate refers to the amount of scrap recycled at its end of life in a product divided by the total amount of waste plus reused metal. For carbon steel, today it is about 60% of the global average, that is, 60% of all scrapped steel is used again in new products. Recycled fraction refers to the scrap content in new products, and this number is approximately 33%. The discrepancy between these two figures comes from the fact that today, and in the coming years, steel demand by far exceeds the available scrap.

Nonetheless, with about 1.1 billion t of steel recycled in 2021, steel is by far the world's most recycled material, a trend that is growing (1). Forecasts suggest that up to 66% of future steel products could be made from scrap by 2050 (**Figure 3**) (44, 45). Yet, projections vary due to the material's longevity in many products (see **Supplemental Figure 2**) (3). Market estimates for 2050 show a range in total production between 2.2 and 2.5 billion t of crude steel per year, and the global share of scrap is estimated to range between 45% (36) and 70% (35, 46) by that time. In either case, one should note that locally the fraction of recycled steel can be much higher, but the aim of reducing global CO_2 emissions requires considering global numbers. Yet, this means that only 45–70% of the steel sector will be circular by 2050.

Supplemental Material >

2. CURRENT CHALLENGES IN SECONDARY STEEL PRODUCTION

Making long products and high-performance sheet steel grades (**Figure 4**) from scrap is associated with different types of challenges for each product and grade. Long products, such as those used in construction, are less demanding in terms of chemistry and microstructure, while the high-performance sheet steel grades are particularly sensitive to chemistry (particularly to the impurity content) and microstructure. When it comes to secondary steelmaking, high-performance steels have stringent requirements for scrap quality due to their low tolerance for chemical contamination and the problem of composition changes from charge to charge. This means that scrap-based high-performance steels require well-sorted scrap and novel alloy concepts that are more impurity-tolerant.

Using steel scrap for long products alone can therefore be regarded as a downcycling process because long products are less demanding with respect to chemical composition and mechanical properties compared with the steels that served (in part) as scrap input. This means that current steel scrap utilization in secondary synthesis is mostly a downcycling process in which steels are converted into products of lower quality and value relative to their original features. The main reason for that is not only the impurity content that intrudes through mixed scrap but also the gradual accumulation of certain hard-to-remove elements upon repeated recycling (**Figure 5**).

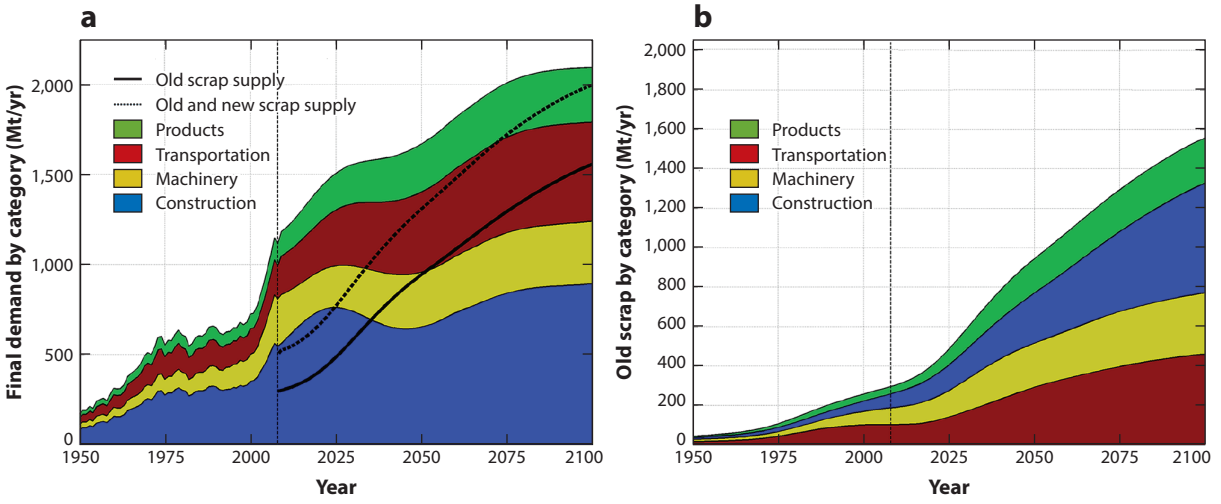

Figure 3

Old and new scrap supply and origin of steel scrap by end-use sector: (*a*) final demand by end-use sector and total scrap supply and (*b*) old scrap supply by end-use sector. The global steel scrap market will grow substantially, by about a factor of two in the next decades (*solid and dashed black lines*). Using more scrap for secondary synthesis is the fastest way to rapidly decarbonize steel production. This could reduce CO_2 emissions by up to two-thirds of total production relative to emissions from the blast furnace route, a goal achievable by 2050–2060. One has to distinguish between old scrap and new scrap. Old scrap, also known as obsolete scrap, is mixed scrap from end-of-life products. New scrap, also known as prime or prompt scrap, is generated during the manufacturing process before being used by an end customer. This also includes material generated internally at a company site during production, such as in steel mills or foundries. This type of scrap usually remains on site for recycling. Note that there are variations in these definitions in the literature. The data show that steel production will not be circular the coming decades due to the 30–60% mismatch between the market demand for scrap and scrap supply and the fact that the majority of the scrap is old (unsorted, contaminated) material, which will likely be downcycled rather than upcycled. This is the main leverage point for basic research, namely, to make new high-performance steels more impurity tolerant. Figure adapted with permission from Reference 45.

Contaminant elements that intrude and accumulate through the repeated use of scrap in steel production are referred to as tramp elements, impurities, or intentionally or unintentionally introduced elements (3, 47–52). These elements can be grouped into several categories (53–56). One category includes elements that are not desired in a specific final product. This can be further subdivided into two subgroups. The first subgroup includes elements that are undesirable in the steel but can be easily evaporated or oxidized to the slag in the converter or in secondary ladle metallurgy. Examples include Si, Mg, Al, Mn, Pb, and Zn. The second subgroup encompasses elements that cannot be readily removed by conventional metallurgical methods, such as Cu, Mo, and Sn (57–60). The total amount of Cu, Ni, Co, Mo, Cr, and Sn is therefore often used as a quality measure for scrap (35, 40, 61). A second major category includes elements that are of value as alloying elements for certain sheet steel products and—if they were not introduced through the scrap—would have to be purchased and added intentionally. This is an approach pursued in alloy-to-alloy recycling (i.e., use of new scrap), where not only Fe but also desired alloying ingredients such as Ti, Cr, Ni, V, and Nb are used on purpose. The challenge is that these two categories cannot be generalized across all steel grades, because whether an element is an impurity or a costly and desired alloy ingredient depends on the target alloy (62) (see also **Supplemental Figure 3**). For this reason, alloy-to-alloy recycling (also referred to as closed-loop recycling), in which alloy scrap is used to produce new alloys of very similar composition, is the best strategy for secondary steel production and for the reuse of valuable elements in the scrap. This requires sort-specific scrap collection.

Supplemental Material >

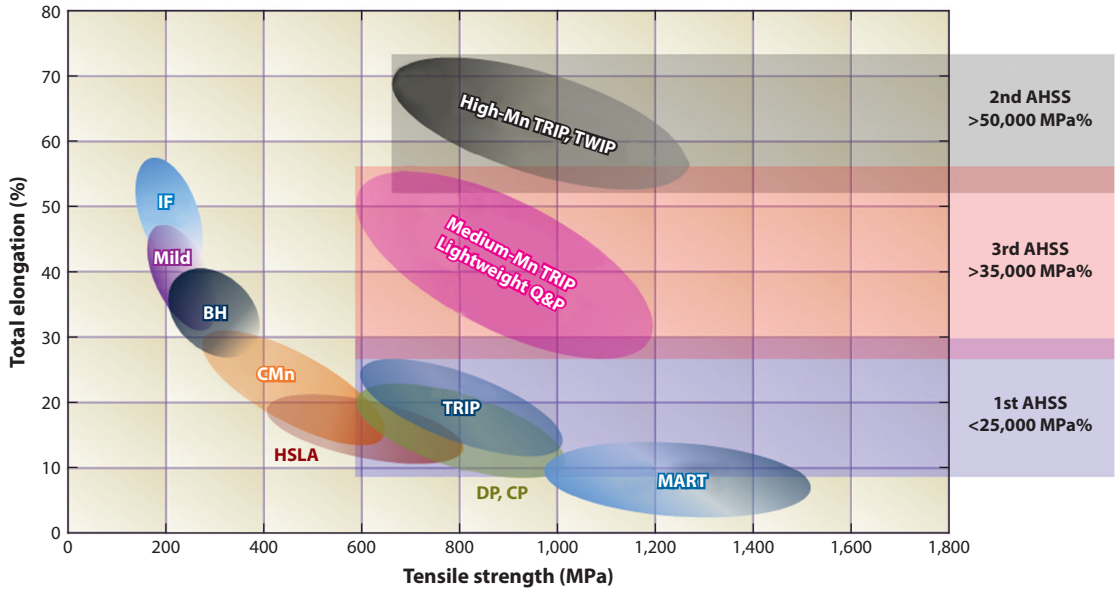

Figure 4

High-performance sheet steel groups. Abbreviations: AHSS, advanced high strength steel; BH, bake hardening; CP, complex phase; DP, dual phase; HSLA, high-strength low-alloyed; IF, interstitial-free; MART, martensitic; Mild, mild steel; Q&P, quench and partitioning; TRIP, transformation-induced plasticity; TWIP, twinning-induced plasticity.

While alloy-specific scrap collection is required to keep a maximum amount of alloy elements in a circular loop, it does not work as a general approach because the majority of the stocks today are, and in the future will be, of mixed postconsumer scrap types (**Figure 3**) (63). An exception is the class of highly alloyed Cr–Ni stainless steels for which scrap sorting followed by up to 90% alloy-to-alloy recycling via EAF melting has been established for decades. Alloy-specific scrap separation is facilitated in this sector because ferritic stainless steels (Cr-based) are ferromagnetic while austenitic ones (Cr–Ni-based) are not. However, alloy-specific scrap sorting is less established for carbon steels: Today, >50% of that market is made of contaminated old scrap, a fraction that is forecast to increase to more than 70% in the next decades (35). Contaminated postconsumer scrap is a material class that is also referred to as mixed, old, or end-of-life scrap (**Figures 3** and **6**). It is the main cause of the ingress of scrap-related impurities.

This increased concentration of impurity elements affects the treatment of the liquid material, casting, and downstream production processes, as well as the microstructure and properties of the final material. This last aspect is of critical importance when producing high-performance sheet steels from scrap. Undesired microstructural effects can include large carbides and nitrides, intermetallic precipitates, nonmetallic inclusions, banded microstructural features, low-melting eutectics, grain boundary and interphase segregation, decohesion zones, partitioning, alteration of protective oxides, and changes in the transformation response and the associated size and shape changes. These important effects explain why most steel scrap today is downcycled into less demanding grades rather than upcycled into high-performance and safety-critical steels. Therefore, most downcycled steel today is used in construction, where about 52% of the world's steel is currently consumed (40).

However, many important and high-value-added products require advanced high-performance steels with stringent requirements for strength, corrosion, toughness, ductility, fatigue, creep,

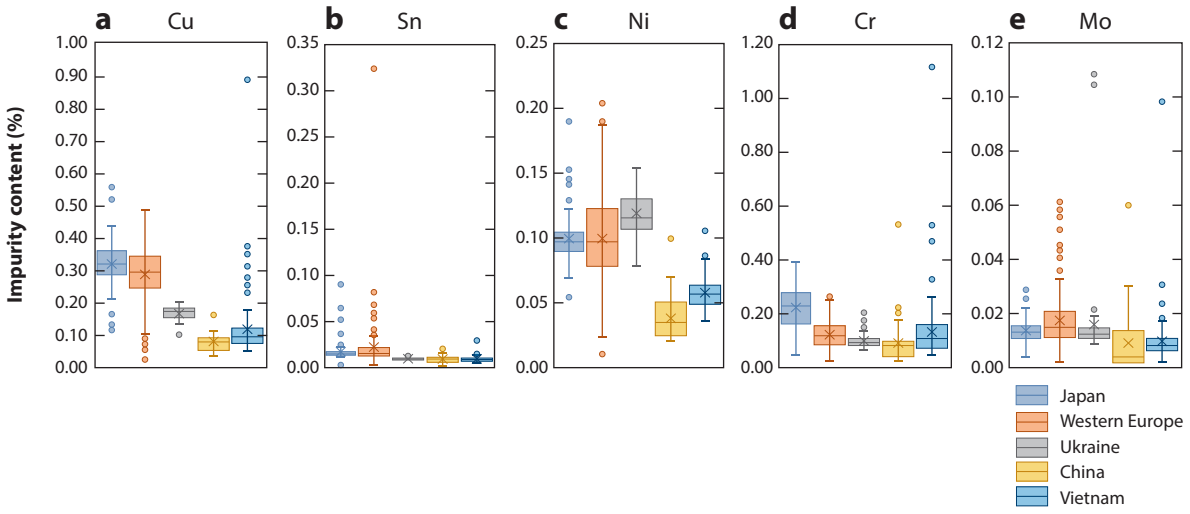

Figure 5

Contaminant elements in steel scrap used for secondary synthesis in several selected regions: (*a*) Cu, (*b*) Sn, (*c*) Ni, (*d*) Cr, and (*e*) Mo. Figure adapted from Reference 47 (CC BY 4.0).

cryogenic response, and/or resistance to hydrogen embrittlement (64–72). Such steels are needed, for example, in the transportation, energy conversion, infrastructure, offshore engineering, and hydrogen and liquefied natural gas industries (2). This means that downcycling alone is not a suitable approach for a sustainable turnaround in the steel industry. Rather, researchers must study which metallurgical measures can be developed to upcycle steels from contaminated scrap into high-grade materials for highly demanding and safety-critical applications.

In this context, improved composition-specific sorting of scrap is an important engineering task. A few commercial options exist, and their implementation is often a matter of cost, such as with more chemically sensitive online composition probing (such as via laser-induced breakdown spectroscopy and gamma neutron activation analysis) and artificial intelligence (AI) methods that can automatically differentiate between different types of alloys through a variety of simultaneous characterization and machine-vision-based techniques (48, 73, 74).

In contrast, the metallurgical challenges associated with secondary production and the effects of contaminants on the microstructure and the processing of high-performance sheet steels have received less attention and often lack scientific foundation. Therefore, this article explores the thermodynamic, kinetic, and microstructural aspects of high-performance steels made from mixed scrap. Some main categories in this field include the following:

1. methods for cleaning and refining the contaminant-affected liquid steel using techniques from ladle metallurgy, vacuum degassing, argon stirring, and slag metallurgy, as well as blending (also called sweetening) strategies between secondary feedstock (variable scrap of diverse origin) and primary feedstock (pig iron, direct reduced iron, converter steel, EAF steel);
2. scrap-specific adjustment of processing steps such as near-net shape sheet production (thin slab casting, strip casting), hot rolling, cold rolling, annealing, and quenching; and
3. the effects of contaminants on thermodynamics, kinetics, microstructure, and properties (the focus of this article).

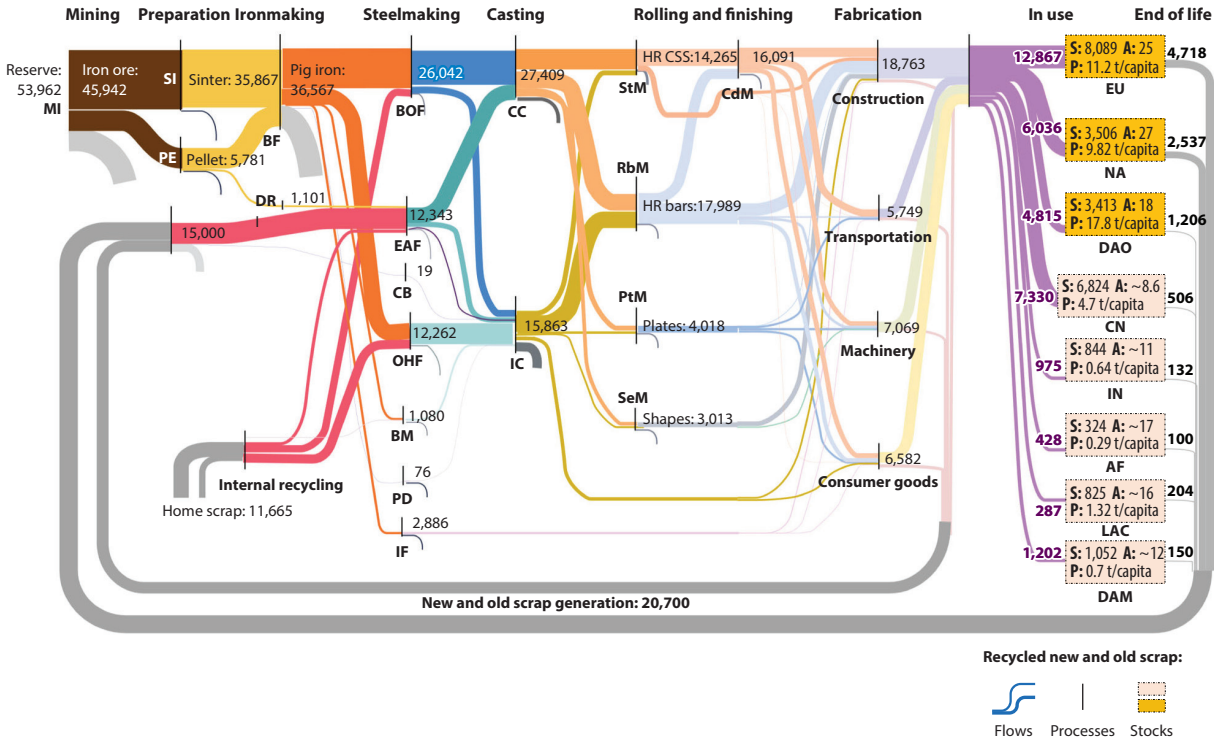

Figure 6

Sankey flow diagram for old and new steel scrap, with numbers representing millions of tonnes. Abbreviations: A, average age of existing stock in years; AF, Africa; BF, blast furnace; BM, bar mill; BOF, basic oxygen converter; CB, crucible; CC, continuous casting; CdM, cold rolling mill; CN, China; CSS, carbon capture and storage; DAM, developing Asia and Middle East; DAO, developed Asia and Oceania; DR, direct reduction; EAF, electric arc furnace; EU, European Union; HR, hot rolling; IC, ingot casting; IF, iron foundry; IN, India; LAC, Latin America and the Caribbean; MI, mining; NA, North America; OHF, open hearth furnace; P, stock; PD, puddling; PE, pelleting; PtM, plate mill; RbM, rod bar mill; S, stock amount in millions of tonnes; SeM, section mill; SI, sintering; StM, strip mill. Figure adapted from Reference 32 (CC BY 4.0).

The second and third categories are closely connected because thermomechanical processing as well as modified alloy and microstructure concepts can offer opportunities to mitigate, repair, or even avoid harmful effects from impurities and cope with their ladle-to-ladle variation by adjusting the subsequent rolling or heat treatment. The latter point refers to the problem that using high scrap fractions causes not only impurity accumulation but also impurity differences among charges due to variable scrap composition.

3. RECYCLING CAPABILITIES AND TECHNOLOGY FOR SHEET STEEL SCRAP SORTING FROM THE AUTOMOTIVE INDUSTRY

Sheet steels are key materials for the automotive industry, with a global market share of about one-sixth of all sheet metals (75). However, when counting only highly formable and high-strength sheet steels, automotive products comprise >85% of the global market share (75). Sheet steels in this sector are mostly collected and recycled, reaching end-of-life recycling rates as high as 90–95% (76). However, today these materials are mostly not collected and recycled in an alloy-specific manner but rather are downcycled instead of upcycled into new high-performance sheet

Table 1 Overview of the main high-performance steel groups used for manufacturing sheet materials for automotive forming applications with typical chemical composition ranges in wt%

Steel type	Steel grade	C	Si	Mn	P	S	Al	Ti	Nb	Cu	Other elements
IF	CR160IF	≤0.01	<0.3	<0.60	<0.06	<0.025	>0.010	<0.12	≤0.09	<0.20	NA
IF-HS	CR210IF	≤0.01	<0.3	≤0.80	<0.08	<0.025	≥0.010	<0.12	≤0.09	≤0.20	NA
HSLA	CR420LA	≤0.12	≤0.5	≤1.65	≤0.03	≤0.025	≥0.015	≤0.15	≤0.10	≤0.20	NA
BH	CR210BH	≤0.08	≤0.5	≤0.70	≤0.085	≤0.025	≥0.015	NA	NA	≤0.20	NA
DP	CR440Y780T-DP	≤0.18	≤0.80	≤2.90	≤0.05	≤0.010	≥0.015 −1.000	Ti + Nb ≤ 0.15		≤0.20	Cr + Mo ≤ 1.40; B ≤ 0.005
Low-C TRIP	CR450Y780T-TR	≤0.25	≤2.20	≤2.50	≤0.05	≤0.010	≥0.015 −2.000	Ti + Nb ≤ 0.20		≤0.20	Cr + Mo ≤ 0.60; B ≤ 0.005
CP	CR570Y780T-CP	≤0.18	≤1.00	≤2.50	≤0.05	≤0.010	≥0.015 −1.000	Ti + Nb ≤ 0.15		≤0.20	Cr + Mo ≤ 1.00; B ≤ 0.005
MS	CR860Y1100T-MS	≤0.13	≤0.5	≤1.20	≤0.02	≤0.025	≥0.010	Ti + Nb ≤ 0.15		≤0.20	Cr + Mo ≤ 1.00; B ≤ 0.010

Abbreviations: BH, bake hardening; CP, complex-phase; DP, dual phase; HS, high strength; HSLA, high-strength low-alloyed; IF, interstitial-free; MS, martensitic steel; NA, not applicable; TRIP, transformation-induced plasticity.

steels (3). The reason lies in the chemical complexity and wide variety of steels used today within a single vehicle. A body-in-white structure contains parts of quite different steel grades, such as high-strength low-alloyed (HSLA), bake hardened, dual-phase, complex-phase, transformation-induced-plasticity (TRIP), twinning-induced-plasticity (TWIP) and mild steels (**Figure 4**) (77, 78). Each steel class has a specific microstructural design, which is responsible for its specific forming and strengthening features, enabled by delicate chemical and microstructure tuning (**Tables 1** and **2**) (79–82). This is required, for instance, for adjusting austenite (meta)stability, martensite start temperature and hardness, ferrite strain hardening, recrystallization, or bainite transformation kinetics, to name but a few aspects (64, 70, 71). The narrow admissible impurity content for these adjustments makes it challenging to use a mixed scrap because vehicles are largely recycled by compacting partially disassembled car bodies with mixed materials, which are welded, glued, and bolted together (75).

The major challenge of secondary steel production therefore lies in the often unknown and variable chemical composition of the input scrap. This means that the achievable type and composition of the steel depend on the respective batch of the mixed scrap that serves as input (83, 84). This also comes from the fact that each car manufacturer uses different steel types for individual components. Additional impurities come through the adjoining of nonferrous material in vehicles. These can be aluminum alloys, coatings, solders, galvanic platings, electronic components, and so on. Various studies have indicated that the accumulation of Cu and Sn is a particular issue because these elements are hard to remove from the melt by metallurgical processing (3, 47, 49, 53, 85–87). Additionally, the adaptation and advancement of multimaterial concepts (88) and the rise of electric vehicles (89–92) make recycling even more challenging because the material mix and the degree of material–design integration are even more intense in these vehicles. This is particularly due to the higher fraction of electrical and electronic components that are likely to remain encased together with steel scrap when disassembly is either not simple enough or not cost-efficient. It is clear that proper separation and sorting of automotive components will be crucial to sustaining the current recycling flow and to reducing the downcycling fraction for the next generation of automobiles (3, 90, 91, 93).

Table 2 Overview of the main high-performance steel groups used for manufacturing sheet materials for automotive forming applications with ranges of mechanical properties

Steel grade	Yield strength (MPa)	Ultimate tensile strength (MPa)	Total elongation in uniaxial tensile test (%)	Strain hardening exponent (*n* value)
Mild 140/270	150	300	38–44	0.23
BH 210/370	210–240	350–380	32–41	0.18
BH 280/400	320	421	30–34	0.16
IF 260/420	280–310	420–520	30–48	0.20
DP 300/500	350	520	30–34	0.16
DP 350/600	390	640	24–30	0.19
DP 400/700	450	730	19–25	0.14
DP 500/800	520	835	14–20	0.14
DP 800 – DP 1000	650–750	800–1,000	12–17	0.09
HSLA 350/450	360	470	23–27	0.16
HSLA 490/600	510	630	20–25	0.13
HSLA 550/650	590	676	19–23	0.12
TRIP 350/600	400	630	29–33	0.20
TRIP 450/800	550	825	26–32	0.24
TWIP 450/1000	500	1,102	50–54	0.41
CP 800/1000	840	1,000	8–13	0.11
CP 800 – CP 1200	650–750	800–1,200	8–13	0.11
MS 950/1200	960	1,250	5–7	0.07
MS 1100/1500	900–1,000	1,100–1,500	4–6	0.02–0.07

Yield strength and strain hardening show up to a ±8–15% variation in the literature. Abbreviations: BH, bake hardening; CP, complex-phase; DP, dual phase; HSLA, high-strength low-alloyed; IF, interstitial-free; MS, martensitic steel; TRIP, transformation-induced plasticity; TWIP, twinning-induced plasticity.

The most critical impurities are Cu and Sn (47, 62, 94) as well as alloying elements from special steels, namely Cr, Mn, Mo, and Ni (62, 86, 87, 95, 96). The latter elements are less problematic in terms of their potential influence on the properties of high-performance sheet steels after recycling and more in terms of their value that is lost upon downcycling (3, 90, 91, 93). With improper sorting and mixing of various steels, the effective loss of these elements (in the sense that they do not contribute to the properties of low-grade sheet steels) can be as high as 93%. Ohno et al. (62, 94) have demonstrated that through proper separation and sorting, inherent value losses can be significantly reduced to only a few percent, which, however, requires meticulously designed separation processes (47, 85). This could be achieved through car construction that facilitates disassembly through inverse engineering. If material-specific separation techniques are employed, the detrimental agglomeration of Cu and Sn in the scrap could be reduced to an acceptable level. This can be further supported by introducing additional preprocessing of scrap, which could help to dilute and extract Cu effectively. Some of these measures require legislative guidance for the set-up of design and recycling processes (90).

When steel scrap gets mixed with contaminated metal from other industries, further elements such as W and Co can enter the scrap stream. These elements, similar to Sn and Cu, cannot easily be extracted from melts in conventional metallurgical processes (3, 33, 87). Excessive addition of W and Co can significantly modify the machinability and malleability of the steels. Additionally, in the case of high-carbon steels, W can lead to brittle carbide formation that can cause cracking during rolling and reduce fatigue resistance. Although several other alloying elements, such as V,

Ti, Nb, B, Si, and Al, can be introduced to secondary steel through improper recycling, they can be removed through proper slag processing and extraction (87).

An alternative to conventional upcycling consists of collecting highly alloyed steels and extracting the valuable elements as Fe–X binary precursors or more complex prealloyed mixtures. These master alloys could directly serve as a secondary feedstock for certain subgroups of steels. This approach can be sensible in secondary synthesis because it is often not necessary to decompose scrap into individual elements but instead into certain master alloys, saving the energy and CO_2 emissions associated with full elemental recovery. However, the majority of recycled steels today are chemically relatively lean Fe–C alloys. They can be the alloy basis for either recycled high-performance sheet steels or conventional long products, provided they are not contaminated by Cu. This can be further supported by novel processes for purifying specific elements, such as C, from steel scraps (97). This process can be particularly interesting for the transition from older to newer generations of high-performance sheet steels.

A more general approach is to develop unified classes of chemically lean steel groups, in which different processing and heat treatment techniques are used to tailor the microstructures toward specific property requirements (1, 3, 48, 87, 98–100). This approach replaces chemical variation with microstructure variation and is also referred to as the uni-alloy concept (48, 99, 100). Thanks to its multiple equilibrium and nonequilibrium transformations and resulting microstructure types, steels are particularly suited for this, as evidenced by the hundreds of variants that can be realized by using only Fe, C, Mn, and Si. This amounts to replacing much of the chemical variability with microstructural variability. However, this approach is not a solution for the gradual accumulation of impurities through the scrap, which means that recycling of vehicles still requires component separation and/or chemical treatment to reduce Cu and Sn in steel scrap.

It is clear that separation is the main limiting factor for high recycling yield and increased upcycling capability of high-performance sheet steels. From this perspective, when compacting and shredding are the only options for preprocessing of the scrap, then sophisticated separation is needed. Through the advancement of recycling and separation of various materials in the waste industry, there is a growing set of techniques available today (28, 94, 101). Machine-vision-enhanced shape detection in conjunction with in situ chemical probing coupled with thermomechanical and magnetic separation methods supported by AI learning algorithms could be a pathway to efficient scrap separation (54, 73, 102, 103). This would have a twofold effect. First, precious alloying elements and base materials could be separated from low-grade materials and be used for upcycling of steels or for use in industries with demand for specific alloying elements (for instance, Ni and Cr for battery applications). Secondly, it could eliminate energy-intensive and environmentally challenging processes for downstream element extraction. However, even with such separation solutions, a certain amount of impurity elements will prevail in the scrap. For this reason, better understanding of the influence of the main impurity elements on the thermodynamics, kinetics, microstructure, and properties of high-performance sheet steels is essential.

4. GENERAL CONSIDERATIONS FOR SCRAP-RELATED IMPURITY EFFECTS ON SHEET STEELS

Several groups have reviewed the influence of some of the most important scrap-related impurity elements on several main property categories of carbon steels (47, 49, 54–56, 104–107). The most important results from these papers, as well as further considerations on the influence of these elements on thermodynamics, kinetics, microstructure, and phase transformation behavior, are discussed in this section, placing focus on (*a*) upcycling strategies and (*b*) Fe–C-based high-performance sheet steels (52, 60, 108–117).

Table 3 Classification criteria for the influence of scrap-related impurity elements on the microstructure, processing, and properties of advanced high-strength sheet steel

Thermodynamics	Associated effects on kinetics, microstructure, and properties	Examples of elements with strong influence
Segregation and partitioning coefficients during solidification	Influence on Scheil segregation and on the resulting inhomogeneity of composition and microstructure	Sn, C, As, Sb, Mn, C, Si, Ni
Equilibrium and nonequilibrium phase transformation temperatures (e.g., martensite start and end, delta-ferrite-austenite, austenite-ferrite, Curie temperature)	Equilibrium and nonequilibrium phase transformation and associated microstructures, local driving forces for phase transformation, transformation kinetics (e.g., martensite start temperature, pearlite formation, bainite formation), etc.	C, N, Si, Mn, Ni, Co, Mo, Cr
Vacancy formation energy	Diffusion coefficients, transport mechanisms, (hydrogen-enhanced) embrittlement effects, creep	H, C, Mn, Cr, Mo
Elements that are hard to remove from liquid steel mixtures	Remain mostly in the liquid metal and can promote brittleness and corrosion	Cu, Sn, Mo, N, W, Ni, Co
Element partitioning in the liquid (metallic melt/slag) and in the solid among adjacent phases	Slag formation, nucleation, interface energies, drag forces, damage, fatigue	Si, Ca, Al, Mn, C
Adsorption isotherm	Grain boundary and interface segregation	B, C, Sn, N, Sb, As, Mn, Ni, Cr, P
Element solubility in the solid and liquid phases	Solid solution strengthening; change of stacking faults (energy, Suzuki segregation) and dislocation cores; thermal activation barriers for glide, cross slip, and vacancies; nucleation effects; resistivity; interface drag forces (impurity drag)	C, N, H, Mn, Cu, Si, P
Phase formation (precipitation including microalloying, low-melting phases, intermetallic phases)	Precipitation kinetics, shape, and size; embrittlement; hot cracking; interface drag forces (Zener drag)	W, Ti, Nb, V, Zn, Al, Cu, Sn, Pb, C, N, B, Cr, Si, Mn, Ni
Stacking fault energy	Twins; stacking faults; martensitic transformation; Suzuki segregation; strain hardening; double cross slip; dislocation nucleation; dislocation recovery; primary, secondary, and tertiary recrystallization; grain growth; nucleation; deformation-induced martensite formation (ε, α')	C, N, Ni, Mn, Co, Cr, Si, Al
Chemical nobility	Corrosion, slag formation, galvanic element formation	Cr, Cu, Si, C, Mn, Al, Ni, As
Slag basicity	Viscosity, partitioning, melt protection, foaming	Ca, Si, Al

We discuss these topics using the categories listed in **Table 3**. Chemical similarities among some of the elements are discussed to identify subgroups of specific contaminants that cause related effects in the melt, slag, solidification, or microstructure. Examples include groups of elements that act similarly on the solidification interval and Scheil segregation, the size and shape of the austenite or ferrite (α, δ) phase fields, the stacking fault energy, corrosion, slag foaming, or interface segregation. A specific example of a contaminant group that has an effect on the phase transformation of ferritic steels is Cr, Mo, Si, and As, which all enlarge the ferritic phase field, while elements such as Ni, Co, Mn, Sb, C, and Sn enlarge the austenitic phase field and affect (mostly reduce) its stacking fault energy.

Some elements are discussed in detail below with regard to their expected gradual accumulation in postconsumer steel scrap due to their rather high nobility. Examples include Cu, Pb, Ni, Sn, and Mo, all elements that are hard to remove from the melt (53, 57, 85, 118). This means that the effects they cause on the microstructure and properties through their enrichment in steel after repeated recycling require taking corresponding countermeasures (56, 57, 95).

Other alloying elements can be grouped because they reduce the diffusion rate of C in ferrite and austenite. This is important for steels made from high scrap fractions because this affects practically all transformation phenomena, microstructural constituents, and properties including strength, toughness, corrosion embrittlement, and welding. It is important to note that the majority of the elements that intrude through scrap delay the formation of pearlite and bainite and thus influence the critical cooling rate as well as the martensite start temperature. Cr and Mo are particularly relevant in that context because they shift the pearlite start to higher temperatures and at the same time lower the bainite formation to lower temperatures, leading to a larger transformation-inert region. The reduction of the critical cooling rate for martensite formation has the consequence that this athermal transition is generally facilitated, but on the other hand, continuous hardening is made more difficult by the decreasing martensite start and finish temperatures with increasing impurity content. Interestingly, the C content is less of an issue here because steel scrap today has a moderate content (about 0.05–0.3 wt% C) compared with the near-eutectic pig iron used in primary production. As a result, using steel scrap as feedstock allows for a more rapid drop in C content during steelmaking.

Most of these impurity-related effects act on the microstructure, and only a few of them are also highly relevant for the electrochemical behavior, that is, corrosion. Better understanding of the effects of impurities on the microstructure is particularly essential for steels because the huge success of this material class is not due to expensive alloying but to its complex microstructural cosmos. Therefore, impurity elements pose a serious challenge for the microstructure-centered design approach that has made steels so successful over the centuries. Hundreds of steels are produced with a very limited spectrum of only 4–6 alloying elements in small quantities (often <1 wt%), yet a huge range of properties is realized (64) (**Figure 4**).

This observation suggests that scrap-based steel design should adopt a philosophy in which maximum microstructural complexity can be realized with chemical simplicity (1, 98). This implies that chemically lean uni-alloy steels should not differ much from one another in terms of their bulk chemical composition but instead differ in terms of their microstructural local element partitioning and properties (3). While the chemical composition is a conserved quantity, the microstructure is not and can thus be renewed over and over again by suitable solidification, deformation, and heat treatment protocols. This qualifies C steels on the one hand as chemically well-matching donor materials for melting new steels from their scrap and on the other hand as acceptor alloys that can be mass produced from other C steels. However, while this lean-chemistry benefit makes steels very sustainable, once the material has been synthesized, it also makes them vulnerable to impurities and their charge-to-charge variation. The reason is that many of these impurities can have a significant effect on the microstructure in small doses because they can shift considerably (in part by orders of magnitude) the equilibria and kinetics, which govern the many equilibrium and nonequilibrium phase transformations that are usually behind the versatile microstructure–property relationship.

The discussion in the ensuing sections of the metallurgical effects summarized in **Table 3** is conducted along several main questions: (*a*) Which problems do these elements cause during processing? (*b*) What are the main contamination pathways, that is, where does the scrap that carries these impurities come from? (*c*) How do these elements behave in the liquid state (metal

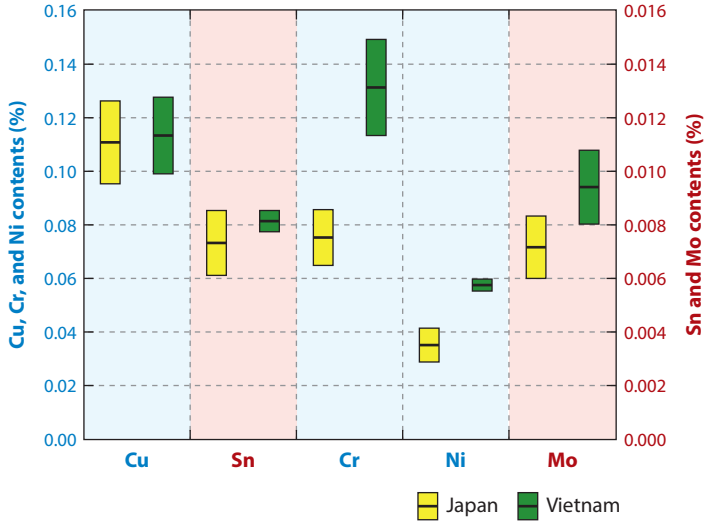

Figure 7

Tramp element analysis for scrap-contaminated steel long products (bars), considering the important impurity elements Cu, Sn, Cr, Ni, and Mo. The impurity analysis differentiates between such elements that enter in long product C-steels used in Japan (*yellow*) and comparable C-steel products from pre-treated Japanese scrap. The bottom and top of each box show a 90 percent confidence interval for the mean, which is indicated by the line inside the box. Figure adapted with permission from Reference 49 (CC BY 4.0).

melt, slag), and how can they be removed? (*d*) Which effects do these elements leverage in the solid state, and how do they alter the microstructure and properties?

As an example, Daigo et al. (49) conducted a study on steels made from scrap that considered 15 contaminant elements. Altogether, 89 steel bars were screened for impurity levels and changes in uniaxial yield stress, tensile strength, tensile elongation, weldability, and fracture toughness. For establishing impurity-oriented property and process control the authors suggested a holistic approach considering scrap sorting and element-specific recovery, the production process, the microstructure, properties, and performance (**Figure 7**). Their findings on the main effects of contaminants on steel properties are summarized in **Table 4**.

Table 4 Main effects of contaminants on steel bar properties

Property	Mn	Cu	Cr	Si	Ni	P	S	Mo	As	Sn	Co	B	V	Ca	Al
Tensile strength	+	+	+	+	+	+	NA	+	+	+	+	+/−	+	No	+
Elongation	−	−	−	No	−	−	−	No	NA	−	NA	+	+	No	+
Yield point or proof stress	+	+	+	+	+	NA	NA	+	NA	NA	NA	+/−	+	No	+
Soundness in the welding area	−	−	−	−	−	−	−	−	NA	NA	NA	+/−	−	NA	NA
Fracture toughness	+/−	−	+/−	+	+	−	−	+/−	−	NA	NA	−	+	+	+/−

Plus signs indicate a positive effect, negative signs represent a negative effect, and both signs (+/−) indicate either a positive or a negative effect depending on the steel type. "No" means there is no significant effect. Abbreviation: NA, not available. Data from Daigo et al. (49).

5. THERMODYNAMIC AND KINETIC SIMULATION OF SCRAP-RELATED IMPURITY EFFECTS

5.1. Basic Considerations

Thermodynamic databases are essential tools for alloy design and materials processing. To use them in the current context they need to cover alloying (Mn, Al, Cr, Ni, Si, C, N, B) and contaminant (Zn, Cu, H, P, S) elements. Each of these elements contributes differently to the stability of the Fe-rich solutions [liquid, ferrite, austenite, and epsilon (ε-martensite)] and second-phase precipitates, which may deteriorate or enhance properties and processability. Even more important for steelmaking, these different elements have different affinities for O, which affects their ability to be removed from molten steel. The objective of this section is to present some important types of thermodynamic and kinetic calculations that can guide the design of steel compositions and processes with larger amounts of scrap. We intentionally choose examples that are relatively simple in terms of alloy composition for educational purposes. However, we must keep in mind that state-of-the-art computational thermodynamic software can handle complex multicomponent systems, such as those encountered in commercial alloys and slags. The examples were calculated using the software Thermo-Calc (119) with the TCFE13 database for steel and iron alloys (120) and the TCOX12 database for metal slag and oxides (121).

5.2. Equilibrium Calculations

The first step to calculate the equilibrium state of a system is to define its condition in terms of thermodynamic variables. These can be extensive or intensive variables (i.e., whether they scale with the amount of the components or not). Intensive variables that must assume uniform values in the whole system at equilibrium are called potentials. Temperature, pressure, and the chemical potential of a component are examples of potentials. We cannot define a system by setting a potential and its conjugate extensive variable at the same time. For example, we cannot define the volume of the system and at the same time define the pressure of the system. The activity a is a convenient representation of the effective concentration of a given component in a mixture and is related to the chemical potential μ_i of the component i by the equation (122)

$$a_i = e^{\frac{\mu_i - \mu_i^\theta}{RT}},$$

where μ_i^θ is the reference chemical potential of the component, R is the gas constant, and T is the absolute temperature. For ideal solutions, the activity of a component is equal to the concentration of a component, and for an ideal gas, the activity of the species referred to as the gas phase at the same temperature is equal to the partial pressure of this species.

Equilibrium calculations are useful for understanding a specific material or process to the extent that the defined system conditions reflect the actual case. For example, **Figure 8** shows the equilibrium volume fraction of phases as a function of temperature for a Fe2%Mn0.3%Cu (wt%) steel composition. This system was defined at constant pressure (1 atm) and as isothermal at each point of calculation along the x-axis. The system is assumed to be chemically closed, and, therefore, we can define the system size as constant and define the percentages of Mn and Cu as constant. The calculations show that austenite (face-centered cubic) is the only stable phase between 823°C and 1,428°C. These calculations seem to suggest that this temperature range is a suitable window for hot rolling of the material and that 0.3 wt% Cu will not cause major problems during processing. Nevertheless, as we show below, this is an incorrect conclusion since the role played by the formation of an oxide scale cannot be neglected.

Figure 9 gives a more detailed picture of the situation. This system was again defined at constant pressure (1 atm) and temperature (1,200°C), but its size was not defined as constant since

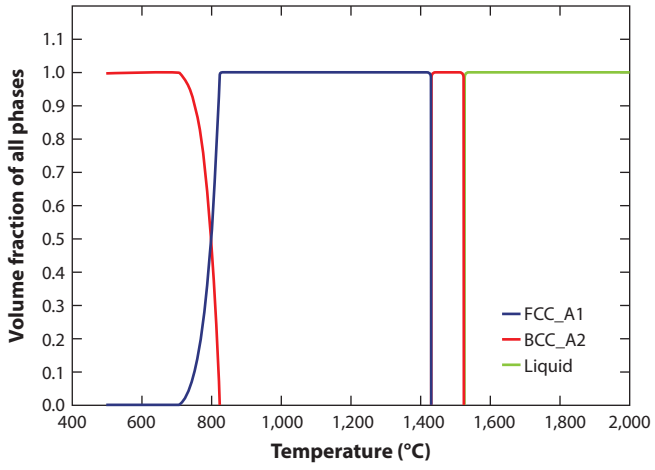

Figure 8

Equilibrium volume fraction of phases as a function of temperature for a Fe2%Mn0.3%Cu (wt%) steel composition. Abbreviations: BCC_A2, ferrite; FCC_A1, austenite.

we would like to know the equilibrium state of the system open to a given partial pressure of oxygen (O_2). Therefore, the initial steel composition is defined in terms of the amounts of Fe, Mn, and Cu (in grams or the equivalent in moles), giving the targeted Fe2%Mn0.3%Cu (wt%) alloy. The oxygen content is defined by the activity of O_2 in the gas phase, which is equivalent to the partial pressure of O_2 for an ideal gas. The results allow for a closer analysis of the problem. Since the partial pressure of O_2 is approximately 0.21 atm, the outer layer will oxidize to hematite (corundum phase), and a gradient of the O activity will develop along the oxide scale for kinetic reasons (**Figure 9*a***). Since Cu has lower affinity for O than Fe and Mn, a liquid phase enriched in Cu is formed (**Figure 9*b***). It is worth noticing that the liquid will be more enriched in Cu at the interface between the oxide scale and metal since the O content is lower. This Cu-enriched

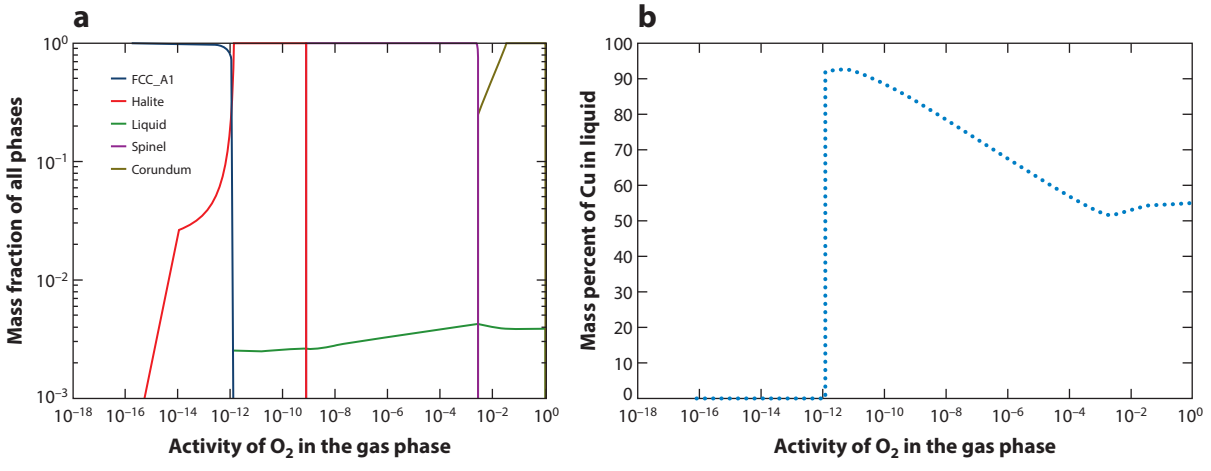

Figure 9

(*a*) Calculated phase fraction as a function of the oxygen potential at 1,200°C for a Fe2%Mn0.3%Cu (wt%) steel composition. (*b*) Mass percent of Cu in the liquid as a function of the oxygen potential at 1,200°C. Abbreviation: FCC_A1, austenite.

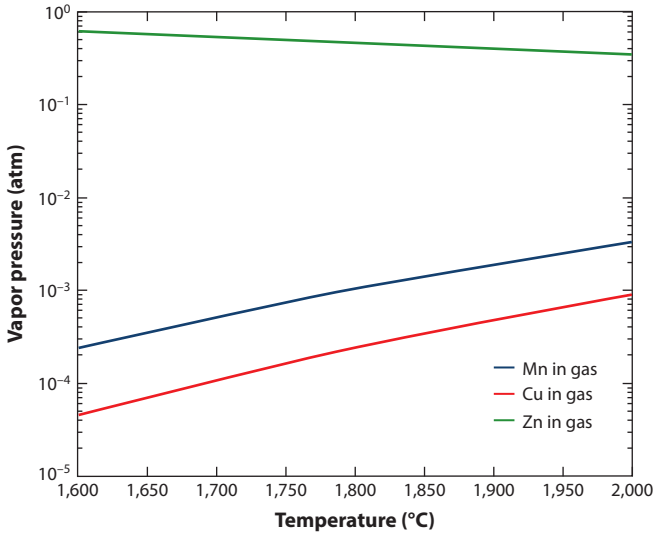

Figure 10

Equilibrium vapor pressure as a function of the temperature of Mn, Cu, and Zn, assuming a Fe0.5%Mn0.5%Cu0.5%Zn (wt%) steel composition and 1 atm of total pressure.

liquid penetrates the austenite grain boundaries under stress during hot rolling and forging, causing surface cracking, an effect known as hot shortness (111, 123, 124).

The same principle discussed above can be used to calculate equilibrium vapor pressures or the equilibrium partial pressures of the various species in the gas phase, which equilibrates with the composition of a liquid or a solid. The temperature at which the equilibrium vapor pressure at the surface of a liquid becomes equal to the pressure exerted by its surroundings is called its boiling point (125). Evaporation takes place when a condensed system is open to an external atmosphere (open system), but the equilibrium vapor pressures are not reached at the external atmosphere. If a liquid or solid is kept inside a closed container (closed system), the atoms or molecules do not have the chance to escape to the surroundings. Boiling, on the other hand, occurs within the condensed system in the form of bubbling (in the liquid) or formation of pores (in the solid). The equilibrium partial pressure of a given species in the gas phase can be obtained by the product of the activity of this component in the gas phase and the total pressure. **Figure 10** shows the equilibrium vapor pressure as a function of temperature of Mn, Cu, and Zn, assuming a Fe0.5%Mn0.5%Cu0.5%Zn (wt%) liquid steel composition (the gas phase is not stable within the closed system at this total pressure and range of temperature). Zn has a higher vapor pressure than Cu by several orders of magnitude. As a consequence, unlike Cu, Zn can be easily removed by evaporation during steelmaking, but corresponding Mn losses due to coevaporation must be taken into account when adjusting the alloy composition.

Thermodynamic calculations can also be used for a first rough estimate of the energy required for a given process. **Figure 11** shows equilibrium calculations for a 1 t Fe 0.40 wt% Cu system initially at 25°C. The system's pressure was defined as 10 Pa to reflect the pressure in vacuum induction melting or vacuum arc remelting furnaces. The enthalpy of this system was varied, and the temperature evolution and the phase fractions are shown in **Figure 11*a*,*b***. The temperature reaches a plateau above 1,600°C where the gas is formed. The mass percent of Cu in the liquid as a function of the system's enthalpy is plotted in **Figure 11*c*,*d*** together with the amount of liquid and the volume of the gas. These calculations support previous reports in which high

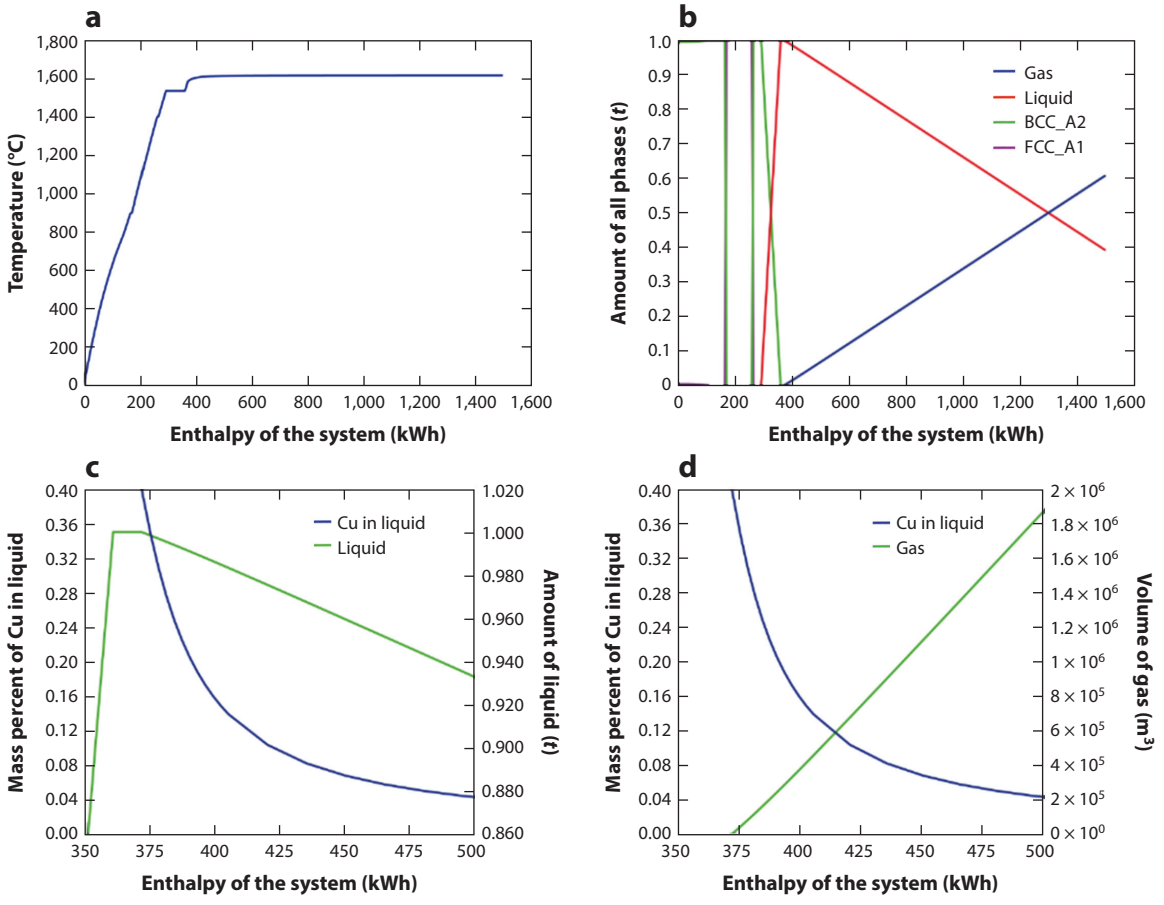

Figure 11

Equilibrium calculations for a 1 t Fe 0.40 wt% Cu at 10 Pa and initially at 25°C. (*a*) Temperature evolution as a function of the enthalpy of the system. (*b*) Amount of phase as a function of the enthalpy of the system. (*c*) Mass percent of Cu in the liquid and amount of liquid as a function of the enthalpy of the system. (*d*) Mass percent of Cu in the liquid and volume of gas as a function of the enthalpy of the system. Abbreviations: BCC_A2, ferrite; FCC_A1, austenite.

vacuum melting in electric furnaces can effectively reduce the amount of Cu present in steels (**Figure 12**). Nevertheless, this procedure would require a massive amount of energy, which is prohibitive for large-scale steel production (53). Also, one must consider that these calculations are a lower-bound estimate of the energy consumption. In reality, energy consumption will be much larger to maintain low pressure, and several remelting steps may be required.

5.3. Scheil Simulations

The Scheil–Gulliver model is used to describe solute redistribution and constitutional undercooling during solidification, that is, the decrease of the melting temperature due to the redistribution of solute between solid and liquid. It is based on three main assumptions (120), namely, that (*a*) diffusion in the liquid phase is infinitely fast, (*b*) diffusion in the solid is zero, and (*c*) the liquid/solid interface is in thermodynamic equilibrium. In classical Scheil simulations, the temperature is decreased step-by-step. When the temperature drops below the liquidus temperature,

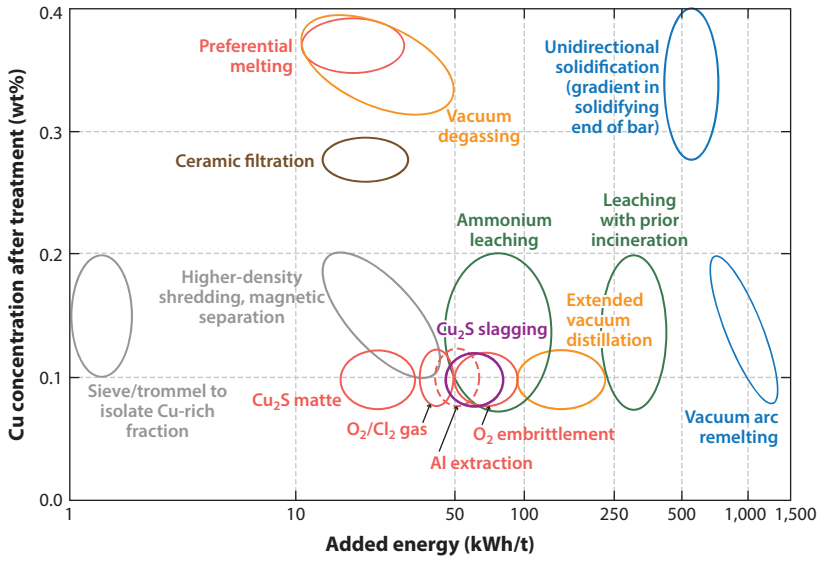

Figure 12

Cu concentration reduction from 0.4 wt% and estimated specific energy consumption for the various processes defined in Reference 53. Figure adapted from Reference 53 (CC BY 4.0).

the equilibrium amount and composition of the solid and liquid phases are calculated. The solid phase is removed from the system, and only the amount and composition of the liquid phase are used for the next calculation step at a lower temperature. Again, the equilibrium amount and composition of the solid and liquid phases are calculated, and again, the solid phase is removed from the system for the next step. This procedure is repeated until the last liquid disappears. This calculation procedure is equivalent to assuming that there is no diffusion in the solid phase and infinitely fast diffusion of all elements in the liquid phase. However, in materials with interstitial elements, such as C, ignoring diffusion in the solid causes large discrepancies with experimental results because of their fast diffusion rates. The assumption of no diffusion in the solid steel during solidification is thus not correct for many cases. Therefore, an improved Scheil model for fast diffusers was developed. This model variant adds the assumption of infinitely fast diffusion of the elements defined as fast diffusers in the solid phase, while the other elements are assumed to have zero diffusion in the solid phase.

The Scheil simulation with back diffusion in the primary phase quantitatively takes into account the real back diffusion of all elements in the primary solid phase (typically the face-centered cubic or body-centered cubic phase) (120). This model requires the use of both a thermodynamic and a mobility database. The calculation also requires the cooling rate to be specified because a fast cooling rate allows for less time for back diffusion, and the simulation result is similar to the classic Scheil–Gulliver simulation. A very slow cooling rate allows for almost complete back diffusion. The simulation is then close to an equilibrium calculation. It also requires that the size of the solidification domain is specified. In most cases this domain size corresponds to the secondary arm spacing, as this is where typically the liquid is trapped during solidification.

In the context of steelmaking, Scheil simulations are valuable tools to understand the redistribution of the solutes during solidification and to design the subsequent processing of the steel. **Figure 13*a*** shows a classical Scheil simulation for a Fe 2%Mn 0.2%C 0.25%Cu 0.02%Sn (wt%) steel composition, assuming C as fast diffuser. As a consequence of solute redistribution, the

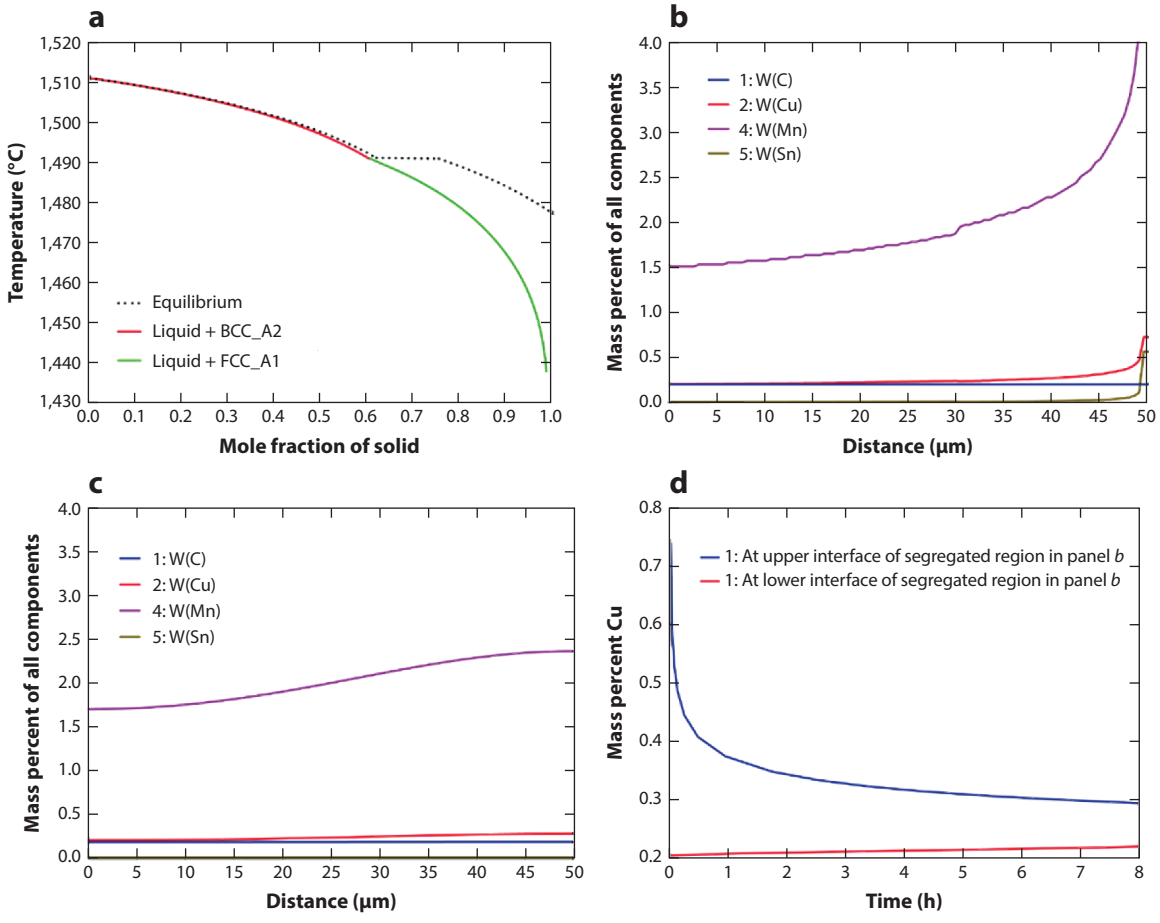

Figure 13

(*a*) Classic Scheil simulation of a Fe2%Mn0.2%C0.25%Cu0.02%Sn (wt%) steel composition assuming C as a fast diffuser. (*b*) Simulated segregation profile exported to the Diffusion Module (DICTRA) in Thermo-Calc, assuming a 50 μm secondary dendrite arm spacing. (*c*) Simulated composition profile after 8 h of homogenization at 1,200°C. (*d*) Simulated mass percent of Cu at the upper and lower interfaces of the segregated region displayed in panel *b*. Abbreviations: BCC_A2, ferrite; FCC_A1, austenite; W, weight percent.

solidification interval is approximately 50°C larger using the Scheil model as compared with the equilibrium case. Higher solidification intervals typically translate into higher crack susceptibilities. In recent years, Scheil simulations have been successfully coupled with diffusion simulations by assuming that the composition of the solid phases estimated using the Scheil model is spread over the estimated length of the secondary dendrite arm spacing. **Figure 13*b*** shows the simulated Scheil segregation profile from **Figure 13*a*** exported to the Diffusion Module (DICTRA) in Thermo-Calc, assuming a 50 μm secondary dendrite arm spacing. This analysis helps us understand that some elements, such as Mn, Cu, and Sn, partition to the liquid during solidification; therefore, the last liquid portion to solidify will contain larger amounts of these solutes. Besides its capability to reveal such microsegregation trends, this profile can be used as an input to a diffusion simulation in order to estimate the time and temperature required for alloy homogenization. **Figure 13*c*** shows the simulated composition profile after

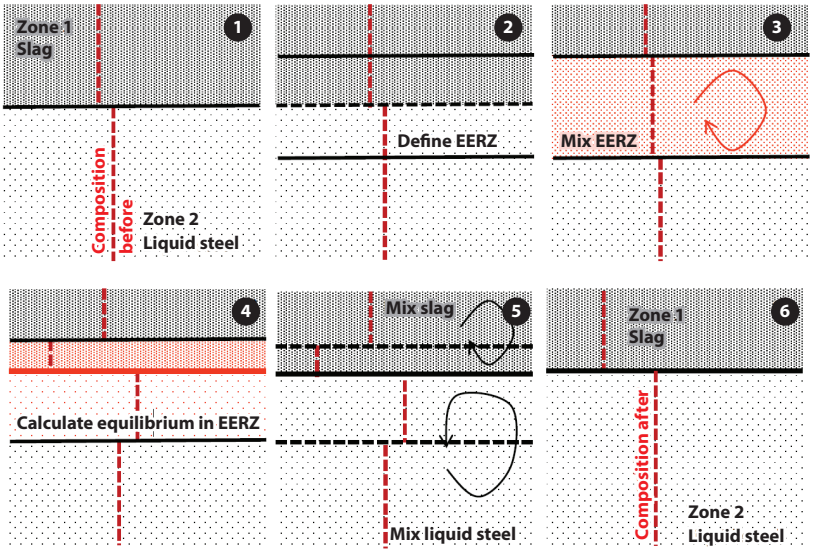

Figure 14

General principle of the effective equilibrium reaction zone (EERZ) model (126, 127), which introduces kinetics to the simulation of a metallurgical process.

8 h of homogenization at 1,200°C. It is apparent in the graph that the composition is still not completely homogenized. We can best visualize the inhomogeneity of the composition over time by plotting it at different positions as a function of time. **Figure 13*d*** shows the simulated mass percent of Cu at the upper and lower interfaces of the segregated region displayed in **Figure 13*b***. The Cu composition remains significantly inhomogeneous even after extended annealing times, and the regions more enriched in Cu are more prone to hot shortness (111).

5.4. Effective Equilibrium Reaction Zone Model Simulations

In recent years, a simple but effective model termed the effective equilibrium reaction zone (EERZ) has been developed (126, 127) and widely applied to simulate the kinetics of various metallurgical processes, such as the ladle furnace (LF) (128), the basic oxygen converter (129), or the EAF (130). The EERZ model is schematically shown in **Figure 14** and has the following steps.

1. The initial situation is a liquid steel (steel zone) and slag phase (slag zone) next to each other but not in equilibrium.
2. An EERZ is defined, encompassing a fraction of the liquid steel phase and a fraction of the slag phase. This fraction of the whole system is assumed to reach equilibrium during a given time step. The size of the zone determines the kinetics. A large EERZ results in fast kinetics and a small EERZ in slow kinetics. The factor defining the size of the EERZ is thus mass transport to and from the reaction zone.
3. The bulk chemical composition within the EERZ is calculated.
4. Equilibrium phase fractions, compositions, and temperatures within the EERZ are calculated.
5. The equilibrium oxide phases in the EERZ are mixed with the rest of the slag phase, and the metallic phases in the EERZ are mixed with the rest of the liquid steel.

6. A new liquid steel and slag composition is achieved that is closer to equilibrium. In the next timestep, the cycle restarts at step one.

Here, we explain this model using the LF as an example. In the electric steelmaking route, scrap is melted under oxidizing conditions in an EAF, although other iron sources, such as direct reduced iron (DRI) or hot metal, can also be charged into the EAF. In the converter route, hot metal from a blast furnace and scrap is transformed into steel in a BOF by blowing oxygen onto the hot metal, thereby removing carbon from the hot metal by oxidation to CO/CO_2. In both cases, the steel is then tapped into a ladle and deoxidized using elements with a high affinity to O, such as C, Si (Si-killed steel), or Al (Al-killed steel). Most often, the ladle is then transferred to a LF for refining. The main functions of the LF lie in the adjustment of the final steel composition through charging alloy additions, heating using an electric arc to control the temperature, buffering for synchronization with continuous casting, improving steel cleanness by promoting nonmetallic inclusions to float up and be absorbed into the slag by bubbling gas through porous plugs in the bottom of the ladle, controlling inclusions by alloy additions (for example, transforming solid Al_2O_3 inclusions into liquid inclusions by adding Ca), and transferring unwanted tramp elements (most notably S) originating from the raw materials used in steelmaking out of the liquid steel into the slag. It is important to note that S can be transferred to the slag only under reducing conditions. This is the reason why this process must be done in the LF. P, the other important tramp element, can be oxidized and transferred to the slag only under oxidizing conditions, meaning that dephosphorization must be done in the BOF or EAF before the steel is tapped into the ladle.

The LF operation parameters published in Reference 131 have been used to set up a kinetic simulation of the LF process using the EERZ model to simulate the behavior of various elements in the liquid steel. Model parameters, such as the mass transfer coefficient to the steel-slag reaction zone, inclusion flotation rate, and efficiency of the electric arc, have been fitted to the steel, slag chemistry, and temperature. **Figure 15*a*** shows how the simulation reproduces the measured steel chemistry as a function of the processing time and process parameters given in Reference 131. The amounts of some elements, such as Mn, essentially depend on the ferroalloy addition: Upon addition of ferromanganese, the Mn content in the steel increases in a step-like function, with the rate increase depending on the melting rate of the added ferro alloy. Note that in this simplified simulation, melting and mixing were assumed to be instantaneous. The variation of other elements is more gradual and depends on the reaction kinetics in the LF. The Al content increases sharply upon the addition of Al with a 20 min processing time but then gradually decreases. This is due to the flotation and absorption of the corundum (Al_2O_3) inclusions that formed by the reaction with oxygen dissolved in the steel into the slag. The rate of the Al drop depends on the flotation rate. Note that what is plotted here is the total Al content, meaning that it can either be dissolved in the liquid steel or be present as a nonmetallic inclusion. Likewise, it is total O that is plotted. Dissolved O is on the order of 2–10 ppm. The S content also decreases gradually. Desulfurization is driven by the partitioning of S between steel and slag. This is governed by thermodynamics and is a function of temperature, O partial pressure, and slag chemistry. The rate is determined by the reaction kinetics between steel and slag, aspects that can be captured by the EERZ model. The gradual Si pickup by the liquid likewise depends on reaction kinetics between steel and slag. The Si originates from the SiO_2 in the slag and is driven from the slag to the steel by the sharp reduction of O partial pressure in the liquid steel upon addition of Al with a 20 min processing time. The amounts of P and Cu, which were additionally considered in this simulation but are not mentioned in Reference 131, remain essentially unchanged. As already mentioned, dephosphorization requires oxidizing conditions and must be performed during steelmaking in the EAF or BOF. Nothing can

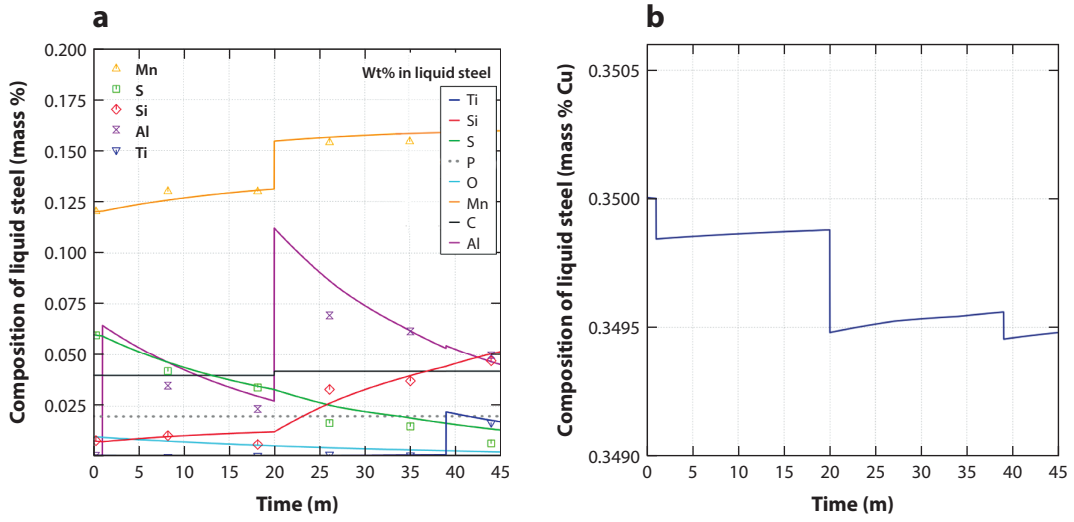

Figure 15

(*a*) Steel composition as a function of processing time in the ladle furnace (LF). Compositions change sharply when additions are made in the LF, then vary gradually as the system slowly moves towards equilibrium. (*b*) Cu content in the liquid steel as a function of processing time. The Cu content of the scrap was assumed to be 0.35 wt%. It remains essentially unchanged throughout the LF process. The tiny jumps in Cu content are due to minimal dilution effects upon the addition of ferroalloys that are assumed to be free of Cu. Again, as for P, the Cu content remains essentially unchanged. No method for Cu removal is currently industrially viable (53), although plasma treatment has recently shown some promise (12, 14). Cu is more noble than Fe such that it cannot be oxidized into the slag. It also does not form sulfides or phosphides stable enough to form a slag. Unlike Zn, it does not have a high vapor pressure to render it into the gas phase. The only option today is to sort and screen the scrap, removing items that contain Cu, such as electric and electronic components, or to dilute the charge with virgin material based on iron ore that is very low in Cu, as discussed in more detail in Section 6. This qualifies Cu as one of the most pressing problems for a circular steel economy.

be done to significantly reduce the P content in the liquid steel under the reducing conditions that prevail in a LF.

Figure 15*b* shows the Cu content as a function of processing time. Again, as for P, it remains essentially unchanged. The slight changes are due to dilution effects upon addition of scrap that is free of Cu. Today, no method for Cu removal is industrially viable (53), although plasma treatment has recently shown some promise (12, 14). Cu is more noble than Fe, so it cannot be oxidized into the slag. It also does not form stable enough sulfides or phosphides that could form a slag. Unlike Zn, it does not have a high vapor pressure to render it into the gas phase. The only option today is to sort and screen the scrap, removing items that contain Cu such as electrical and electronic components, or to dilute the charge with virgin material based on iron ore that is very low in Cu, as discussed in more detail in the next section. This qualifies Cu as one of the most pressing problems in a circular steel economy.

6. CONTAMINANTS IN SCRAP: ORIGIN, REMOVAL, AND EFFECTS ON STEEL QUALITY

6.1. Copper

Cu is one of the contaminant elements that accumulate in steels during repeated recycling. It enters postconsumer steel scrap through brass, bronze, coatings, plating, cables, and engine parts from electrical gadgets and vehicle scrap, as well as electrical and electronic waste (**Figure 16**). Automobile shredding in particular is a growing source of Cu (17, 21). Automobiles contain

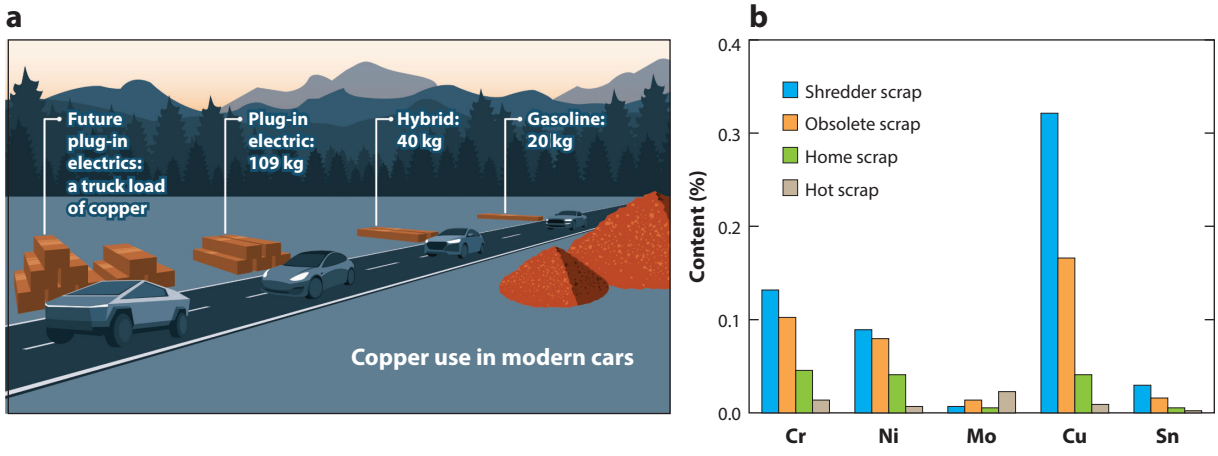

Figure 16

(*a*) Increasing use of Cu in vehicles (3). (*b*) Industry data obtained from scrap analysis confirming this trend (116). Panel *a* adapted from Reference 3 (CC BY 4.0). Panel *b* adapted from Reference 116 (CC BY 4.0), using data from Voest-Alpine Linz AG, originally reported by Preßlinger (131a).

approximately 0.2 wt% Cu, which is trending upward (**Figure 17**). This trend will accelerate due to the growing share of electric vehicles, which have up to five times higher Cu content compared with combustion vehicles (see also **Supplemental Figure 4**) (53, 54, 85, 132). Cu is also used in some grades as an alloying element, such as in soft magnetic and weathering steels, materials whose market fraction is growing. In high-performance sheet steels, Cu is not used as an alloying element but instead is an impurity (22, 40). This constraint particularly applies to sheet steels for forming operations (92, 133). In Japan, two-thirds of the currently accumulated Cu content in scrap is due to insufficient scrap separation, and only one-third is inherited from steel with Cu as an alloying element (49). Daigo et al. (49) screened steels made from scrap for the Japanese market for 15 different impurity elements, focusing on long products. The Cu levels observed were particularly high, with an average value between 0.25 and 0.5 wt%. This accumulation has

Supplemental Material >

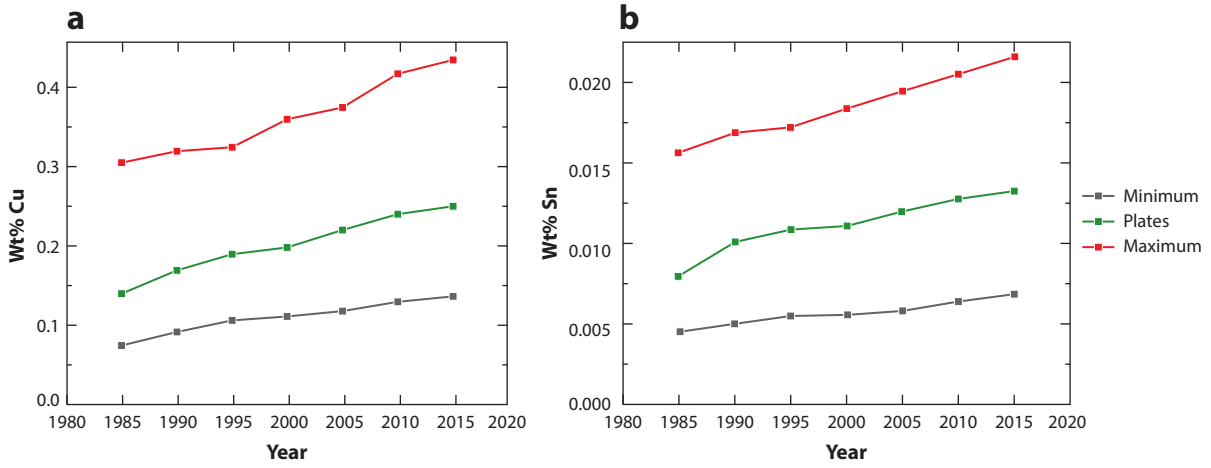

Figure 17

Increase in (*a*) Cu and (*b*) Sn contents in steels. Figure adapted from Reference 105 (CC BY 3.0).

Supplemental Material >

a negative impact on the quality of recycled steel and is expected to result in restrictions on recycling in the future (47, 49, 53, 58, 134, 135). The total content of Cu, Sn, Cr, Ni, and Mo is even used as an indicator for scrap quality (59, 136). While material flow studies reveal the likelihood that such tramp elements accumulate (**Figure 5**) (see also **Supplemental Figure 3**), knowledge of their impact on properties and possible microstructural mitigation strategies is scarce.

Daehn et al. (85) showed that globally over the long term, the expected levels of Cu contamination will require recycled steel to be used exclusively in products with a higher Cu tolerance (e.g., reinforcing bars) and that the demand for this scrap will be lower than the supply, assuming that scrap is freely traded for optimal recycling (see **Supplemental Figure 4**). In the case of the European market, this trend has been observed since 2009, when the supply of Cu-contaminated scrap exceeded demand, with the remnant quantity exported (136). An effective way to remove Cu from scrap is improved scrap sorting. However, in many cases this is very challenging due to the element's often high dispersion (small Cu-containing parts immersed in bulk scrap) and solid-state integration (coatings, solders, precipitates) in bulk scrap.

Due to its noble character, Cu cannot be readily removed from liquid steel by oxidation. Because of its low vapor pressure, Cu is also difficult to remove using vacuum treatment and thus requires (too-)long treatment times (53). Although a good yield can be achieved with vacuum remelting, this process is not economically viable for sheet steel grades, especially when considering the additional base material lost during such a process. Further theoretical possibilities include the removal of Cu through an H-containing plasma treatment, as a sulfide (137) or as a chloride (138), approaches that have not yet been tested at a commercial scale. The current industrial solution is to use DRI to dilute the Cu-containing scrap in the EAF process, lowering the Cu content in the hot metal below the critical value (e.g., $\leq$0.15 wt% for sheet production). However, this approach is energy- and CO_2-intensive. Also, as explained above, the removal of Cu from the material cycle of scrapped steel is not possible at reasonable cost levels; thus, advanced alloying, microstructure, and processing strategies need to be developed to turn Cu into a less harmful element.

This pathway, however, has been less explored. Once Cu is inside the solidified steel, it is a primary trigger of hot and warm cracking during casting and cooling, hot rolling, hot band coiling, and forging, making it one of the most harmful tramp elements (**Figures 18** and **19**) (60, 111, 118, 123, 124, 139–141). This detrimental effect is also referred to as (surface) hot shortness. For sheet steels, the danger lies in its occurrence during the hot rolling process due to diffusive accumulation of Cu beneath the oxide layer (114). In an oxidizing atmosphere, iron forms a layer of scale on the surface of the slabs, below which Cu can enrich during slab reheating and hot rolling between 1,000 and 1,100°C (142). Like other chemically nobler elements, Cu is not built into the oxide scale but instead partitions into the adjacent phases, heterointerfaces, and grain boundaries. Cu can accumulate to such an extent that it exceeds the maximum solubility in austenite (~9 wt% at 1,250°C) (143, 144). Since hot rolling takes place in a temperature range between 1,000 and 1,200°C, the Cu-enriched subsurface regions can liquefy due to Cu's low melting point (1,080°C) (145). This liquid phase can penetrate the austenite grain boundaries and initiate surface cracks, thus embrittling the product during hot rolling (114, 123).

While the hot cracking phenomenon is the most critical effect associated with the limited solubility of Cu in the oxide scale, it also influences the scaling behavior during high-temperature processes such as hot rolling or forging. Due to the segregation between the scale layer and the metal matrix, the adhesion of the scale is reduced, leading to uncontrolled descaling. Since the scale acts as an insulation layer during hot rolling, helping to maintain the sheet's temperature, unexpected descaling due to chemical variations will cause higher temperature losses between the forming steps, which renders such processes less sustainable and needs to be addressed by process adjustments.

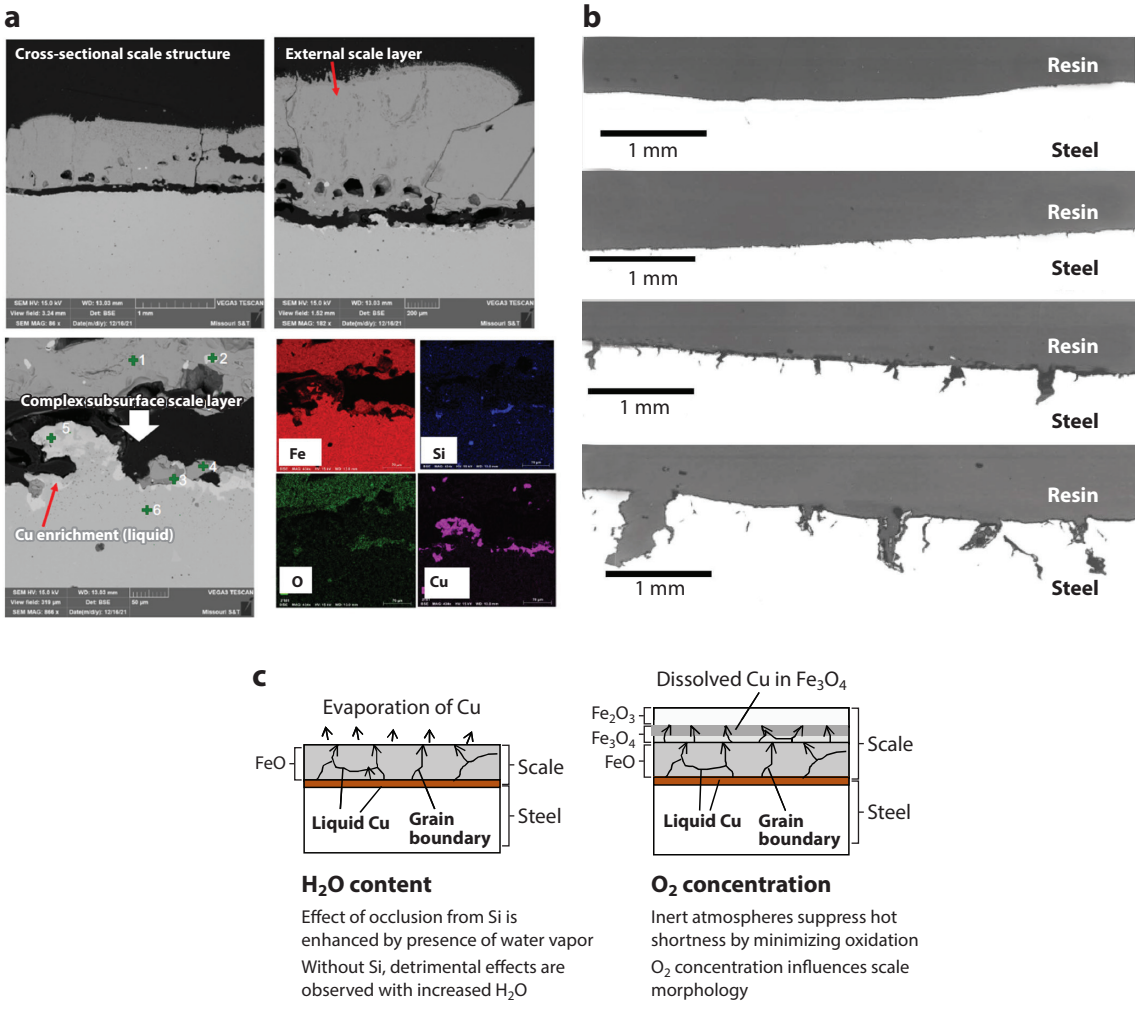

Figure 18

(*a*) Cu accumulation in a scale structure of a high-Cu-containing model steel. (*b*) Hot shortness due to Cu in a model steel with 0.28 wt% Cu after oxidation and uniaxial tensile testing and (*c*) its suggested mechanisms for both the case of the presence of water vapor (*left*) and high-O_2 oxidizing environments (*right*). Panel *a* adapted from Reference 158 (CC BY 4.0). Panels *b* and *c* adapted from Reference 159 (CC BY-NC-ND 4.0).

Thus, changes in the solidification and hot rolling processes could be possible solutions to overcome hot shortness. Rapid solidification via strip and thin-slab casting has been proven to be an effective approach to eliminate the hot shortness introduced by Cu (107, 139). In this approach, due to rapid cooling, the Cu gets finely dispersed as a nanoprecipitate in the matrix instead of forming liquid Cu-rich layers. This can effectively eliminate hot shortness and increase the steel's high-temperature formability. Cu in a metallic solid solution can even lead to nanoprecipitates during annealing, thus refining the grain size and increasing strength.

The addition of Ni is one way to mitigate the harmful effects of Cu. Ni stabilizes austenite and increases the solubility of Cu, preventing its precipitation (104, 110, 118, 147, 148). Yet, this approach is not really viable due to the high costs of this element. In contrast, Sn reduces the

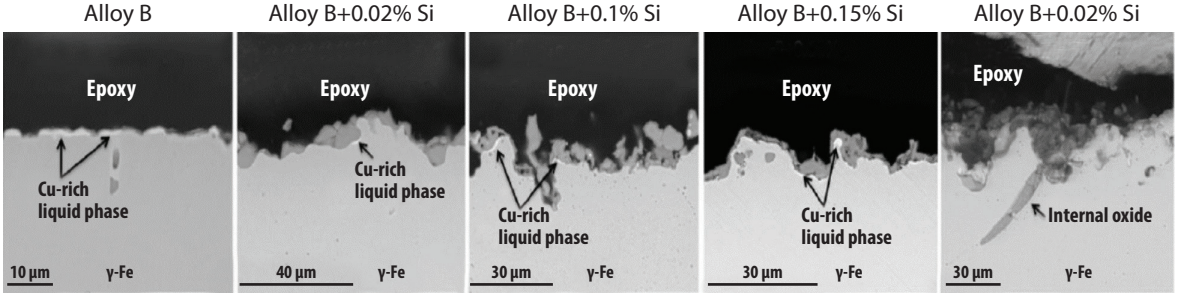

Figure 19

Role of Si in Cu-related hot shortness. Figure adapted with permission from Reference 146.

solubility of Cu in austenite and lowers the melting temperature of the Cu- and Sn-rich phases (149), thus favoring hot and warm cracking. Sb also has a negative influence since it reduces the solubility of Cu in austenite to a similar extent as Sn (150). Kondo and colleagues (123, 151) reported that Si, Mn, S (together with Mn), and B reduce the susceptibility to hot shortness. They suggested that this effect acts by decreasing the amount of the Cu-enriched phase at the steel/oxide interface. Significant occlusion of the Cu-enriched phase into the scale was observed in steels that contain Si (**Figure 19**). Another mechanism that can counteract hot shortness is the addition of P, Si, B, and C, which were assumed to restrain the penetration of the Cu-enriched phase into the grain boundaries. It was observed that higher sheet heating temperatures can reduce hot shortness but at the cost of higher oxidation losses and larger grain sizes, which in turn actually enhance surface hot shortness.

In contrast to these challenges, in some cases Cu also serves as an alloying element, as it improves the weathering resistance of low-alloyed steels. However, these steels will not conquer a market share large enough to take up all the Cu-containing scrap. The soft weathering steels are employed primarily for decorative purposes, and they are not used in mechanically highly demanding sheet products. In acid-resistant high-alloy steels, a Cu content of >1 wt% provides improved resistance to hydrochloric acid and sulfuric acid. In a few soft magnetic Fe–Si steels, Cu has been used to form nanoprecipitates. This increases strength because these phases pin dislocations; however, they do not enhance coercivity due to their small size of a few nanometers, which is below the thickness of the magnetic domain walls (152–157).

Beyond these general trends associated with the uptake of Cu from scrap, the influence of this element has also been studied for high-performance sheet steels. For example, studies on a low-alloy TRIP steel with 0.15%C–1.5%Si–1.5%Mn (wt%) revealed that the mechanical properties can even be positively affected by adding just 0.5 wt% Cu. The Cu-containing TRIP steel possessed higher tensile strength and elongation (817 MPa and 36.4%) compared with the Cu-free steel (727 MPa and 29.2%). The observed increase in strength and ductility was attributed to the increased fraction and different mechanical stability of the retained austenite, which in turn led to a more pronounced TRIP effect. In addition, Cu solution in ferrite results in solid solution strengthening. By further adding 0.4 wt% Ni to such a Cu-containing TRIP steel, the residual austenite content could be further increased by about 9 vol%, since both elements, in particular Ni, enhance the austenite phase field. In contrast, the addition of Cr, in combination with Ni, to such TRIP Cu-bearing steels was observed to result in the formation of a large amount of martensite and a small amount of retained austenite (8.9% and 8.5%, respectively). This caused an increase in tensile strength but at the same time decreased ductility, resulting in a mechanical behavior similar to that of dual-phase steel (161–165). For HSLA steels, Hosseini Far et al. (162,

163) demonstrated that a joint alloying of Cu and Ni (1.48–4.16 and 3.48–7.65 wt%, respectively) combined with an adjustment of the final rolling temperature can increase the yield strength by precipitation hardening. The effects of Cu on interstitial-free (IF) steels have been investigated by Rana et al. (166, 167), who reported retardation of recrystallization as well as grain refinement due to lower austenitization temperatures. In addition to these factors, Cu precipitates can also influence fatigue (168, 169). If their size is <2–3 nm, an increase in the cyclic hardening potential has been reported (168, 170), leading to a higher defect tolerance and finally a higher fatigue strength.

Research on steels with C concentrations >0.2 wt% is very limited (171, 172). For such high concentrations the effects are complex because Cu precipitation is influenced by cementite precipitation. Jung et al. (171) investigated steels with 0.44 and 1.53 wt% C and found that the cementite precipitates introduce an additional nucleation site for Cu precipitates, but in comparison with the coherent nucleation in the matrix, at the cementite Cu nucleates incoherently to the matrix, leading to fewer beneficial effects on the mechanical properties.

Medium-Mn steels (MMnSs) are a potential sink for scrap with high Cu concentrations, which explains some of the recent research interest in Cu-alloyed MMnSs. Similar to TRIP steels, Cu additions increase the stability of the retained austenite, leading to a higher ultimate tensile strength (173) but also to a changed strain hardening response since the austenite requires higher mechanical loads to form martensite. More sophisticated heat treatments have been designed to enable a supersaturation in ferrite even after intercritical annealing, which leads to the precipitation of nanometer-sized Cu precipitates in the ferrite, resulting in increased yield strength (173, 174). It was demonstrated by Elbeltagy et al. (175) that variations in the Cu concentration can be compensated for by a change in the annealing time, making this parameter the adjustment screw to deal with fluctuations in the chemical composition.

Research has so far focused on the design of new high-performance steels with a specific, well-defined chemical composition, including Cu. From a circularity perspective, this is not pertinent as it is undesirable to further increase the amount of Cu in the material flow. Recent studies investigate the influence of increasing Cu concentrations in standard alloys, such as 42CrMo4 (109), but are not aiming for a specific Cu concentration. These standard steels are often used in the automotive industry, and properties as well as chemical compositions are today limited to specific standards. The standard for quenching and tempering (Q&T) alloyed steels specifies the maximum amount of Cu to be 0.4 wt%. However, it has been demonstrated that a modification of the tempering temperature of the 42CrMo4 steel with as much as 1 wt% Cu still allows it to meet industrial requirements, even with such a high Cu content.

6.2. Tin, Arsenic, and Antimony

Sn intrudes into steel scrap mainly through recycling postconsumer tinplate packaging materials. Many of these packaging products use low-C steels, which are coated with a thin Sn layer for protection against corrosion. On average, 4 kg of Sn are used for the surface coating of 1 t of steel in these products (108, 116). Another reason for Sn contamination is machinery parts that contain bronze, a Cu alloy with up to 22 wt% Sn. A further Sn source is bearings in engines, which often consist of hard steels that are coated by bronze, sintered bronze, Al–Sn–Cu alloys, and so on. Similar problems exist for Pb–bronze alloys, so-called gunmetal scrap parts (a Cu alloy with Sn, Zn, Pb, and Ni), and brass (a Cu alloy with Zn and sometimes minor additions of Sn). In some cases, up to 60 kg of Sn have been found per 100 t of steel scrap. However, a relatively small amount of about 20 kg of Sn in a 100-t steel melt would exceed the admissible upper limit value of 0.02 wt%. The element As enters the scrap through bearings and Cu alloys, in which it serves as

an alloying element. Similarly, Sb is used in brasses and Pb-based alloys. In small amounts Sn and Sb can be beneficial for improving the corrosion properties of steels by retardation of the anodic and cathodic reactions that result in increased stability of the oxide layer and reduced pitting potential (176, 177). Both elements are considered detrimental in steels and should preferentially be removed.

The electrolytic removal of Sn from Sn plate scrap is today an industrially adopted technology. In this process, Sn is removed from the surface of the plate materials at ~85°C and condensed on a cathode, which can then be used in the Sn industry. By doing so, the residual Sn in steel scrap can be reduced to values as low as 0.02 wt% (178). However, such a detinning practice is not suitable for old scrap because other tramp elements can affect the electric potential for Sn to be effectively removed by electrolysis.

Sn cannot be effectively removed in the conventional melting and slag process. Sn has not only a very low melting point of only 230°C but also the widest temperature range for its liquid phase among all metals and is therefore also not removable by vacuum treatment. However, Sn can be removed to some extent in the plasma atmosphere of an EAF and ends up in the exhaust gas as dust (52). As for Cu, several theoretical options have been explored for removing Sn, for example, as a sulfide (179), chloride (138), or intermetallic phases such as Ca_2Sn.

Sn strongly segregates during solidification and thus creates detrimental chemical and microstructural gradients, impairing the steel's homogeneity (180). Sn, As, and Sb are low melting elements and detrimental to sheet steels because they promote surface cracks, particularly during hot rolling and when coexisting with Cu (181). Once these elements enter the solidified steels they strongly tend to accumulate at all interfaces, that is, grain boundaries, free surfaces, and phase boundaries (182–185). The segregated amount of these elements increases with their bulk content taken up from the scrap. According to the interfacial decohesion hypothesis by Seah (186–188) and Hondros & Seah (189), the reduction in grain boundary cohesion in ferrite is enhanced by larger segregating atoms. Thus, Sn and Sb should be more detrimental than small atoms such as P and As. Measurements by Grabke and colleagues (180, 190, 191) using Auger electron spectroscopy on Fe–Sn–C alloys indicated that the risk of grain boundary segregation by Sn atoms is low when C and B are present because these elements compete with Sn in segregation but have a higher diffusion constant. This finding suggests that it is conceivable that predecoration and thus grain boundary site passivation by light interstitials might be a strategy to protect the interfaces from Sn and Sb segregation, thus reducing the likelihood of intergranular fracture (192, 193). However, such an approach becomes less effective when the steel contains Mn, Cr, and Ni, as tempering embrittlement was observed in low-alloy sheet steels containing these elements as well as Sn, As, and Sb as impurities. The amplifying influence of Mn and Cr is due to their ability to reduce the chemical activity of C, particularly at interfaces. The enhancement of the embrittling effect of these elements with Ni is due to the reduction in the solubility of Sn and Sb in ferrite and the tendency to form intermetallic compounds.

The effects of Sn, As, and Sb have also been studied for specific sheet steel grades. The strong tendency of these elements to segregate to the grain boundaries has a particularly negative effect on formability. Deep-drawing IF steels, for example, have very low C and N levels ($C < 0.003$ wt%, $N < 0.004$ wt%), which are further scavenged from solid solution using microalloying elements (e.g., Nb and Ti) to form precipitates (194). This eliminates the protective effect of the grain boundary passivation through predecoration with C and N. This fact leaves the undecorated grain boundaries unprotected, turning them into defects that are vulnerable to segregation with Sn, As, and Sb, which in turn can lead to interface embrittlement.

Moreover, grain boundary segregation of Sn, As, and Sb can lead to adverse effects on the texture formation in sheet steels. Deep-drawing properties of IF sheet steels are strongly dependent on the crystallographic texture, that is, the crystal alignment of the grains with respect to the boundary conditions imposed during demanding stretching and deep forming operations. A high perpendicular anisotropy with Lankford values (r values) > 1.25 provide material flow out of the sheet bulk, avoiding rapid through-thickness localization when the sheets are subjected to severe deep-drawing applications such as in typical automotive forming operations. Such high r values are favored by a high-volume fraction of recrystallized grains with their {111} plane normal vectors aligned parallel to the sheet plane normal directions (195, 196). Elemental segregation at grain boundaries can suppress this type of favorable texture formation during the primary static recrystallization. Instead, the formation of the (100)[001] and (110)[001] texture can be promoted, which is desirable in the case of some electrical soft magnetic steel sheets (191, 197, 198) but highly undesirable in steels subjected to forming operations. Hence, prevalence of the (100)[001] and (110)[001] texture components over {111}<uvw> texture components would impair the alloys' deep-drawing properties (199).

6.3. Zinc

Zn enters steel scrap mainly because it is used for galvanization, a process that involves coating steel with a layer of Zn to protect it from corrosion. In the future, the use of more Zn cast parts might enhance the content of this element in mixed vehicle scrap further. Zn is more reactive than Fe, so when the steel is exposed to corrosive environments, the Zn sacrificially corrodes before the underlying steel, providing a protective barrier. Galvanized sheet steel is used primarily in automotive and construction applications. On average, the Zn-coated steel sheets have a Zn content of ~2.8 wt% (108). Zn can also enter the steel scrap through brass parts. Zn causes difficulties in the production of steel and leads to environmental problems. Several groups have described separation routes using air and chlorine mixtures to remove Zn from steel scrap prior to melting in an EAF. Thermodynamics shows that zinc chloride is more stable than its oxide, while the reverse is true for iron. Using a 10:1 air–chlorine mixture, Zn has been shown to be selectively removed from steel at 800°C (200). The reaction products characterized by various analytical techniques confirm the thermodynamic analysis. This process offers an attractive solution for obtaining clean steel scrap and useful chemicals.

Unintentional Zn impurities can affect the properties of sheet steels, including their weldability, toughness, and surface quality. However, small amounts of Zn have also been reported to improve formability and ductility because its addition results in grain refinement. It was also observed in the case of low-alloy steels to enhance hardenability and improve the steel's response to heat treatment.

6.4. Lead

Most iron ores contain only very small amounts of Pb. Usually, the Pb content in steel is <0.01 wt%. However, Pb can be taken up through mixed scrap, for example, through scrapped battery components or machining steels. Lead is more noble than iron but can be easily removed by vacuum treatment due to the large difference in vapor pressure between the two elements. However, this poses a problem for low grades, such as mild steel, which are not refined by vacuum treatments, and therefore this impurity is not separable. Although Pb can theoretically be discharged as finely dispersed metal droplets in the slag or as lead vapor or lead oxide dust in the converter and arc furnace, the process control required for this is not currently used. Pb is an element that is practically insoluble in Fe, both in the liquid phase and in the solid state. It also

does not form any kind of compound with the accompanying alloying elements usually present in sheet steels. In the solid state, it therefore occurs in the form of submicroscopically small metallic particles in extremely fine dispersion.

6.5. Chromium

Excess Cr from scraps enters steels primarily through stainless and heat-resistant steel parts, bearing steels, coatings, and so on. More than 85% of global Cr is used in stainless steels (95). Particularly high amounts of Cr are found in ferritic-martensitic heat-resistant steels used in power plants (about 9 wt%), for the formation of the passivation layer in ferritic and martensitic stainless steel (>12 wt%), and for high alloyed Cr–Ni duplex and austenitic stainless steels. Thanks to the high price of Cr (and even more so of Ni), for decades, stainless steels have been well sorted and recycled separately from C steels to prevent the loss of Cr (and Ni) in the life cycle. Yet, the inadvertent intrusion of stainless steel scrap into C-steel scrap has become an increasing source of contamination of steels produced from high scrap fractions. Most of the Cr gets oxidized into the slag during EAF operation in the oxidation atmosphere and is lost in the slag, which is then also a contaminated product, hampering its downstream usage.

Cr enhances the ferritic phase field, although it must be considered that moderate fractions, <8 wt%, moderately enhance the stability of austenite over the ferrite phase field. Cr lowers the critical cooling rate of steels, thus making them oil- or air-hardenable. Reducing the critical cooling rate required for martensite formation generally increases hardenability and thus improves tempering response. Cr has a detrimental effect on notch impact energy and weldability. Notched impact strength is reduced, but it lowers elongation only very slightly. Weldability decreases with increasing Cr content in pure Cr steels. The tensile strength of the steel increases around 80–100 MPa per 1 wt% Cr added due to precipitation (formation of carbides) and solid solution strengthening. It acts as a strong carbide former, and hence it improves cutting ability, wear resistance, and hot strength. With a simultaneously higher C content, Cr contents of up to 3 wt% increase remanence and coercivity. Through its strong scattering effect for electrons, it reduces thermal conductivity and electrical conductivity.

Some of these aspects were also studied in high-strength sheet steels for automotive applications, such as low-alloyed TRIP steel, MMnSs, TRIP-assisted bainitic ferrite, and quenching and partitioning (Q&P) steels, which possess an excellent combination of strength and ductility due to their complex microstructure. In a low-alloyed TRIP steel, it was found that Cr leads to a deterioration of the final microstructure and mechanical properties, while Cu and Ni had positive effects (201–203). In a Q&P steel with an addition of 1.5 wt% Cr or 1.5 wt% Ni, an increase in the residual austenite content was observed compared with the base alloy. Here, Cr had a larger influence than Ni (204–206).

6.6. Nickel

Nickel enters recycled steel primarily through austenitic and duplex stainless steel parts in the scrap. More than 60% of global Ni production is used as an alloying element in stainless steel (35). Less frequently Ni intrudes into steel scrap through consumer products, such as aerospace components, chemical processing equipment, and marine hardware. Ni is a noble metal that, like Mo, cannot be readily removed from the steel bath. Scrap containing Ni must be carefully separated from other scrap to prevent Ni loss and avoid exceeding its limits in carbon steels.

Ni enlarges the austenitic phase field. It is an important element in many sheet steel types. One effect of Ni is to improve corrosion resistance, particularly in acidic and marine environments,

through the promotion of a stable, protective oxide layer on the surface of the steel, preventing further corrosion. In addition, Ni can also enhance mechanical properties, for instance, through its moderate solid solution strengthening effects and its strong influence on austenite stability and on the stacking fault energy of the austenite. Ni can also improve the low-temperature toughness of steel, making it more resistant to brittle fracture (140, 146, 160).

When considering the influence of Ni additions on low-alloyed TRIP sheet steels, it was found that this element (like Cu) is a strong austenite stabilizer and thus increases hardenability. This fact makes Ni attractive for TRIP steels, which rely on the presence of austenite at room temperature. Thus, deformation-driven austenite-to-martensite transformation can be triggered to promote strain hardening and an excellent combination of high strength and superior ductility. Ni is also attractive to counteract the hot shortness in Cu-containing steels by enlarging the solubility of Cu in austenite (207).

6.7. Manganese

Mn uptake from scrap is currently a point of major concern due to the increasing amount of MMnSs (with a Mn content of 3–12 wt%) that are entering the market (208–213). In the future, low-C steels should be strictly separated from MMnSs, like the separate scrap collection of stainless steels today. The reason is that the Mn content of MMnS is far too high to be tolerated in any low-C steel products. In moderate quantities, Mn is comparably harmless and acts as a good deoxidizing element in the steel bath. However, it also interacts with other contaminants. For example, it binds sulfur in the form of MnS and thus reduces the unfavorable influence of the undesired FeS phase. Excess Mn can be removed from the liquid and turned into slag by sulfur and oxygen.

Mn is an austenite stabilizer and reduces the critical cooling rate and thus increases hardenability (214), even to the extent that martensite formation is achieved by air cooling (215). Yield strength and ultimate tensile strength are increased by Mn addition (216, 217). In advanced high-strength steels, such as medium-Mn and high-Mn steels, Mn is a very important alloying element to stabilize and retain a large amount of austenite at room temperature and to tune its stability against athermal transformation under mechanical loads (211, 213, 218). Such steels undergo very high work hardening assisted by the TRIP and TWIP effects, offering an excellent strength–ductility combination, which is particularly attractive for manufacturing complex and safety-critical parts and energy absorption bumpers for automotive applications (79, 212, 219, 220). In addition, Mn increases the coefficient of thermal expansion, while thermal conductivity and electrical conductivity decrease.

6.8. Titanium, Vanadium, and Niobium

Ti, V, and Nb are used in many high-performance sheet steels as microalloying elements due to their very high effectiveness for grain refinement and for mitigating aging effects (221–226). They are therefore also an important factor in the global steel scrap cycle (see **Supplemental Figure 3**). Similar to high-Mn steels, the best option in a future circular steel economy lies in separating microalloyed scrap from low-C steel scrap to facilitate enhanced alloy-to-alloy recycling. Closed-loop recycling is especially important for Nb and V. While Ti's abundance is around 0.5–0.6%, V and Nb have abundances as low as 0.012% and 0.002%, respectively. Closed-loop recycling is particularly useful for the production of high-quality deep-drawing steels. These elements significantly reduce solute carbon and nitrogen from the ferritic matrix by forming carbides, nitrides, and/or carbonitrides to avoid any aging or serrated plastic flow phenomena. In addition, microalloying exploits the dispersed precipitates for improving strength and strain hardening.

Supplemental Material >

Therefore, mixing such scrap with conventional low-C steel scrap loses these valuable elements that are needed for high-performance sheet steels.

6.9. Molybdenum

Mo is a refractory metal that is intentionally added to, for example, case-hardened steels to improve strength, hardness, and corrosion resistance. Thus, Mo can intrude into recycled steels through corresponding scrap parts (25, 32). Because of its noble character, Mo cannot be readily removed by oxidation from the melt and does not evaporate from the steel bath. Since there are currently few methods to remove Mo from steel scrap, dilution is the only option to limit its content. During solidification, Mo can promote and amplify segregation effects, similar to Cr and Mn. It has a very high segregation coefficient in the range of 0.25–0.63, similar to the coefficients of Cr (0.25–0.9) and Mn (0.28–0.72) (227).

Mo improves the hardenability of steel by reducing the critical cooling rate. When it is in solid solution, it increases yield strength and ultimate tensile strength. It promotes fine grains, reduces tempering brittleness in stainless steels, and has a favorable effect on weldability. Mo also increases corrosion resistance and reduces susceptibility to pitting (228). Mo has a very strong narrowing effect on the austenitic phase field and increases high-temperature strength while scaling resistance is reduced. Despite its beneficial role in the case of hardened and stainless steels, it is considered an undesirable tramp element in many low-alloyed sheet steel grades.

Excess Mo can promote formation of brittle intermetallic phases, alter grain boundaries, and impact heat treatment response (54, 62, 94, 105, 115, 229). Intermetallic compounds such as σ, χ, and Laves phases all have high hardness and brittleness, making sheet steels susceptible to cracking and embrittlement, especially at elevated temperatures. Depending on the C content and processing conditions, Mo can react with C to form carbides such as Mo_2C. Their effect depends highly on dispersion, but due to their high enthalpy of formation values, they often form at high temperatures and are thus coarse, leading to higher brittleness and lower toughness. Also, high contamination levels of Mo lead to reduced weldability due to the formation of hard and brittle intermetallic phases in the heat-affected zone. In scrap-based steel production, variations in Mo content can impact the welding process and the quality of welded joints.

6.10. Silicon

Si has a deoxidizing effect and enlarges the ferritic phase space. Excess Si can be removed by slag metallurgy due to its high affinity to oxygen. In steel, it strongly promotes solid solution strengthening, increasing strength and wear resistance. It also strongly increases the elastic limit; therefore, it is added to spring steels (222, 230, 231). High levels of Si increase scale resistance, acid resistance, and resistance to corrosion and oxidation, but electrical conductivity is lowered. Therefore, Si is used in electrical soft magnetic sheets at up to 3.4 wt% (156, 232, 233). In advanced high-strength steels with retained austenite, Si is an important alloying element to retard carbide formation, thus resulting in C in a solid solution in austenite and enhancing its thermal stability.

The intrusion of Si through the scrap can thus have a significant impact on the microstructural and mechanical properties of the final material. For example, the addition of Si to dual-phase steels can alter the balance of strength and ductility substantially (64, 81, 234–239). Si can also accelerate the recrystallization of ferrite during heating in the intercritical temperature range, which in turn promotes the formation of austenite through accelerated nucleation, followed by grain growth. Addition of Si favors the formation of a homogeneous austenite of higher hardenability, resulting in a higher volume of martensite in the final structure.

6.11. Aluminum

Al usually intrudes through the recycling of scrapped steel parts that contain Al-welded components or coatings (35, 57). For example, some automotive parts and household appliances are made of steel that is coated with Al for corrosion resistance. Excess Al can be removed from liquid steel by oxidizing it into the slag (106, 240). Al_2O_3 is less dense than liquid steel and floats to the surface, where it can be easily removed. However, Al_2O_3 inclusions in steel can negatively affect their mechanical properties. Another way to remove Al from liquid steel is through vacuum degassing. In this process, the liquid steel is placed in a vacuum chamber, where the pressure is reduced to remove dissolved gases and other impurities, such as Al.

Al is a strong ferrite stabilizer, reducing the austenite phase field very effectively. It also has a strong tendency to form AlN nitrides and intermetallic phases. While the former are beneficial phases in some steels when finely dispersed, intermetallic phases are usually less desirable, except in some creep-resistant steels. The ability of Al to scavenge N in steel makes it a useful addition to deep-drawing sheet steels, especially for automotive applications. The simultaneous precipitation of AlN during recrystallization annealing promotes the formation of layered pancake-type microstructures in deep-drawing grades (196, 241). This type of microstructure—when combined with crystallographic {111} texturing—can be used to design deep-drawing steels with high planar Lankfort values. This is an anisotropy factor that quantifies the in-plane over the through-thickness deformation components in sheet materials. A high value represents good deep-drawing properties of metal sheets. In addition, binding N with Al also makes steels resistant to aging effects. Al also increases scale resistance and increases coercivity. In advanced high-strength steels, Al (like Si) retards carbides formation, thus ensuring that a large fraction of austenite can be retained at room temperature.

6.12. Further Elements That Can Enter Through Postconsumer Scrap

Be occurs rarely as a scrap-related contaminant. It can enter through Cu–Be alloys, which are used to make springs, in the scrap. It also can come from Ni–Be alloys, which are very hard and corrosion-resistant materials used in surgical instruments. Be acts very strongly on the constriction of the austenite phase field. It can also lead to precipitation, reducing toughness and ductility. Be strongly deoxidizes and can therefore, in the case of moderate contamination, be eliminated through the slag. It also has a very high chemical affinity to S.

P is an element that usually comes through blast furnace ironmaking and not from scrap. It is a strongly segregating element in steels and must be usually kept below 0.03–0.05% for high-quality steels. P increases susceptibility to temper embrittlement even at the lowest levels. The P embrittlement effect increases with higher C content, with increasing hardening temperature, and with grain size. The embrittlement appears as cold brittleness and sensitivity to impact stress. P can be reduced through dephosphorization techniques such as adding lime-based fluxes during refining or using special dephosphorization agents (243, 244).

Excessive S in the scrap can lead to the formation of brittle iron sulfides, reducing the steel's ductility and impact toughness. It can be removed through desulfurization processes such as ladle refining with lime or Mg-based agents or through Mo addition. Advanced methods like vacuum degassing or slag-metal reactions can achieve lower S levels.

Li is an element that is not classically considered an alloying element in steel. Knowledge about its effects is limited; however, it is known to cause liquid metal embrittlement (245). While large efforts are currently being made on the scientific and industrial fronts to enable a very effective system for the recycling of Li-ion battery systems, it can be expected that in the future some of these systems may end up in the scrap by accident. Due to the less noble character

of Li, it can be expected that the contamination can be extracted by standard steel refinement processes.

7. IMPURITY-TOLERANT PROCESS AND MICROSTRUCTURE DESIGN

The question of how to make recycled C-sheet steels more impurity-tolerant, particularly their microstructures and thus also their properties, during processing and in service depends on the type of tramp elements present, their amount, and the specific type of steel considered (48, 60, 85, 94, 117, 246). Another aspect that deserves consideration is the interplay among different impurity elements and their joint effect on the microstructure and properties as well as the variation of the type and amount of intruded elements from charge to charge, depending on the origin of the scrap used for recycling (98, 117, 247). In this context, it is important to keep in mind that the uptake of the different impurity elements can lead to a range of microstructural changes simultaneously. On the one hand, practically all individual elements almost always cause several effects at the same time, for example, changing the temperatures of their respective phase transformations and their segregation and partitioning behavior. On the other hand, the interactions among the different tramp elements are not linear; that is, they can reinforce each other or mutually weaken and compensate their effects. This means that a corresponding design of the alloys and the casting and forming processes as well as the impurity-tolerant microstructure development requires a fundamental understanding of the physical and chemical effects of these relationships, both for all tramp elements individually and for their interplay. Another aspect of impurity-tolerant microstructure design is to define which kind of detrimental effect has to be counteracted, for example, hot shortness and formation of brittle intermetallic phases or coarse carbides (60, 114, 248–250). Interestingly, some of these impurity effects can be attenuated when reducing the austenite and ferrite grain size because this effect sometimes also translates to a finer dispersion of potentially harmful phases and to a dilution of interfacial segregation effects, that is, to an altogether higher homogeneity of the steel microstructure (70, 104, 204, 208, 251–253).

Another point that deserves consideration is defining groups of tramp elements that behave similarly in the liquid phase, where the main distinction is whether they can be turned into the slag by classical metallurgical means and properly adjusted slag basicity or whether they are hard to remove from the liquid steel because of their nobility (254). Here, specific impurities that cannot be easily removed by the steelmaking process, such as Cu, Mo, Pb and Sn, are particularly important (58, 60, 109). Also, the impurity content of such elements will accumulate in final steel products with an increase in recycling cycles.

A further aspect to consider in this context is how tolerant the microstructure and the properties are, not only to the effects of these tramp elements but also to the variation in their amount between charges. This permanent variability in the intruded impurity content might in the future be a bigger problem than working with higher scrap tolerance alone within constant specifications. In other words, a change in the specification for the impurity tolerance of sheet materials for a given constant tramp element intrusion will probably in the future be less problematic than the prediction of how charge-to-charge variations in their content affect the properties. **Figure 20** gives an example of an analysis of the variation in the Cu content of steel bars that have been produced from scrap in the Japanese steel market (49). Based on such data it might be possible to adjust the sheet steel specifications for a certain mean Cu content, but it will be more challenging to also cope with unexpectedly high amounts of Cu entering through the scrap (109). This means that for safety-relevant sheet steel products, the basis for the material and process design cannot be only to meet the average chemical composition but also to deal with the tails of chemical distribution functions that enter through the scrap.

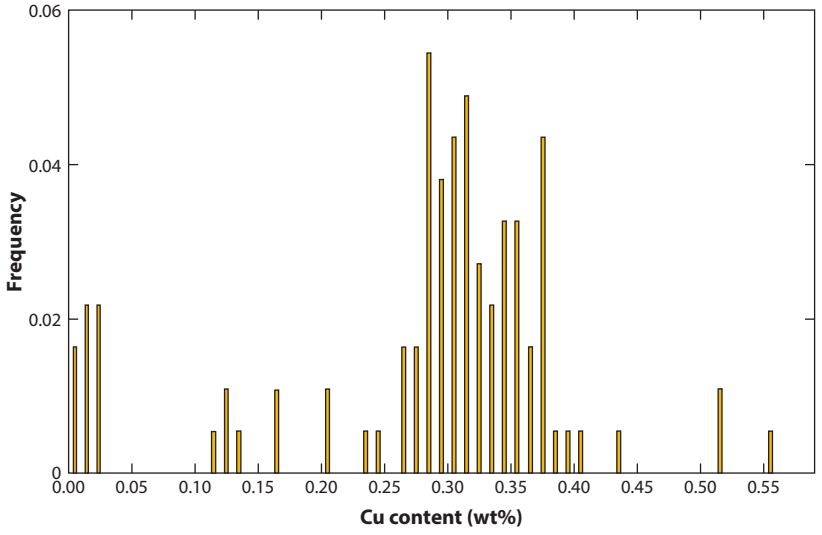

Figure 20

Cu levels measured in steel bars made from scrap in the case of the Japanese steel industry. Figure adapted from Reference 49 (CC BY 4.0).

From a metallurgical perspective, it is important to consider the effect of impurities on thermodynamics and kinetics (**Table 3**) and whether the effect must be predicted under canonical (number of elements conserved) or grand-canonical (chemical potential conserved) boundary conditions. Structuring the different phenomena associated with the uptake of contaminants and their individual and combined effects along these categories provides a knowledge-based approach to derive countermeasure strategies to change the steels' global composition, processing, and microstructures (**Table 5**). Research to identify corresponding countermeasures along these categories, particularly from an alloy and microstructure design perspective, includes approaches such as grain and phase boundary passivation and predecoration (e.g., with C, N, and B), reduction of grain size (particularly of austenite grain size), and codoping in the case of tramp elements that are hard to remove (e.g., adding Ni when Cu contamination occurs) (**Table 6**).

8. CONCLUSIONS AND OUTLOOK

Steel production is the largest single contributor to global CO_2 emissions and hence to global warming. Given the huge size of this sector (1.9 billion t of steel produced per year), the fastest way to decarbonize it is to produce more steel from scrap. A system-related precondition for realizing this is to provide abundant, sustainable, and affordable electrical energy to operate EAFs for upcycling scrap into high-performance steels. Another precondition is to better understand and counteract impurity-related effects on steel processing, microstructure, and properties, particularly in the case of high-performance sheet steels.

While several publications have reviewed the former aspects, that is, the engineering, processing, scrap flow analysis, and efficiency aspects of this approach, this article has focused on the latter questions, that is, the underlying scientific metallurgical questions, placing attention on thermodynamics, kinetics, and microstructure with the aim to better identify research needs for upcycling scrap into high-performance sheet steel.

Table 5 Main effects (negative or positive) leveraged by scrap-related contaminants and possible countermeasure strategies to make carbon sheet steels more impurity tolerant and hence better suited as mass-produced scrap acceptor materials

Effects	Cu	Sn, As, Sb	Zn	Al	Cr	Mn	Ni	Pb	Ti, Nb, V	Mo	Si
Solidification segregation coefficient											
Phase transformation											
Diffusion											
Partitioning											
Grain boundary and interface segregation											
Inverse element solubility in the solid											
Precipitation (intermetallics, carbides, nitrides)											
Corrosion											
Low melting compounds											
Functional properties											

The magnitude of the symbols represents the importance of the effect for a specific tramp element and hence the necessity to control its effects by adequate adjustment of processing and microstructure design as well as by control of intrusion from the scrap.

Table 6 Countermeasure strategies to make carbon sheet steels more resistant to impurities

Target for metallurgical countermeasures against contamination effects	Thermodynamics measures	Kinetic measures
Grain boundaries	Grain and phase boundary passivation and predecoration (e.g., with C, N, and B)	Reduction of grain size (particularly of austenite grain size)
Thermodynamics of phase fields	Codoping for austenite stability tuning in the case of tramp elements that are hard to remove (e.g., adding Ni when Cu contamination occurs), for example, in the case of austenite in medium-Mn transformation (or twinning)-induced plasticity steels	Addition of further elements that can kinetically influence austenite formation
Quenching rates	Co-alloying to change martensite start and end temperatures	Co-alloying to change critical quenching rates, diffusion rates, and nucleation rates
Precipitates	Modify thermodynamic range for precipitates, change precipitates (particularly brittle phases such as sigma phases, Laves phases, certain carbides, interface precipitate films) by alloying	Refine precipitate dispersion by enhancing nucleation rates and faster quenching rates

A few specific conclusions and mitigation strategies are as follows.

- Approximately 60–70% of the steel used for recycling is impurity-contaminated old scrap. This will lead to steels with different chemical impurity profiles compared with the steels that are currently on the market, which are mainly produced via primary synthesis using iron ores.
- Certain elements, such as Cu, Mo, Pb, and Sn, in postconsumer scrap are very challenging to remove from liquid steel. This means that these elements will accumulate over time in steels made from scrap. The consequence is that the scrap quality will decay more and more over the coming decades. This trend will be further accelerated by the electrification of transport, energy, and industry.
- Some specific steel grades, such as certain TRIP steels, soft magnetic Fe–Si grades, and weathering steels, can tolerate larger amounts of Cu-contaminated scrap; however, their production volume is small and not likely to occupy a market fraction in the future that would be large enough to use the potential amount of high-Cu containing scrap.
- There is a need for strategies to generally replace the current downcycling practice (because most C-steel scrap today is used for making construction steels) with upcycling scrap into high-performance sheet steels.
- Upcycling scrap into high-performance steels that serve in high-strength and safety-critical applications requires us to better understand the role of scrap-related impurities by establishing a science of scrap-contaminated dirty alloys and dirty feedstock.
- Studies are needed to investigate and correct (by identifying adequate alloy and microstructure measures) current impurity ranges in steels for a higher amount of scrap use.
- Better understanding the flow of steel scrap, not only in terms of the matrix element Fe but also in terms of the most important alloy ingredients, such as Mn, Si, Ti, and Nb, opens up options for near-alloy-to-alloy recycling and upcycling.
- Closed-loop recycling and composition-specific sorting of steels should be established, following the best practice examples that have been implemented, for example, in the stainless

steel and aluminum alloy sectors. For instance, medium- and high-Mn steel scrap must be strictly separated from conventional C-steel scrap.

- Future scrap sorting must use AI-powered sensing and sorting methods, such as those introduced for aluminum alloys. Scrap yards should be equipped with sensors and internet-of-things devices that collect real-time data on material quantities, quality, and processing rates. These data can be analyzed to optimize operations, predict demand, and streamline logistics. AI in the future can assist in optimizing the entire supply chain, from material collection to processing and distribution. Blockchain technology might ensure the transparency and traceability of materials, certifying their origins and recycling processes.
- Thermodynamic and kinetic knowledge for the removal of Cu, Mo, Sn, Pb, and Zn from steel scrap during pyro-, electro-, and plasma-based metallurgical recycling are urgently needed to establish a scientific foundation to facilitate scrap recycling and, thus, the fast and effective decarbonization of the steel industry. Recent progress in plasma treatment might open up possible pathways for Cu removal from steel melts.
- One option is the design of crossover, broadband, and multipurpose steels to narrow down the chemical range of materials and thus make them more scrap compatible. This must include the question of how to also make scrap-based high-performance sheet steels tolerant to variations in scrap composition from charge to charge. One main approach lies in the refinement of the grain size and the increase in the dispersion of precipitates and segregation profiles. This can be achieved by higher quench rates, more nucleation sites, higher nucleation rates, grain boundary pinning, and grain boundary passivation via predecoration. The former effects can, for instance, be realized through a reduction in the thickness of cast slabs, while the latter measures can be realized by sensitive moderate alloying with suited interface sergeants, a higher recrystallization tendency, and changes in hot band processing.
- Development and application of AI algorithms can facilitate the automated discovery of scrap-related, impurity-tolerant composition–microstructure–process–property relations. Deep learning methods can make processing more dynamically adaptable to composition variations and varying impurity content between different scrap charges.
- Scrap-related steel design approaches are required with the aim to improve the mutual recycling of scrap in new alloys in terms of donor and acceptor concepts.
- Compositionally lean steel design for endless recycling is worth exploring using microstructure-based design as a powerful tool instead of alloying to produce new crossover steels, that is, classes of chemically simple and impurity-tolerant uni-alloy steels. This steel design approach is based on smart microstructure optimization rather than on chemical (over)tuning.
- It is important to aim for the substitution of less sustainable alloying elements in steels with those possessing better sustainability, for example, substitution of Ni by Mn in austenitic, TRIP, and maraging steels.
- Completion and improvement of thermodynamic and kinetic databases for the design and adjustment of steel can help to identify alloy composition ranges with higher tolerances of scrap- and mineral-related impurities.
- Lattice defects in steels can be exploited as (harmless) sites of impurity trapping, for instance, by forming nanoprecipitates for precipitation hardening. This can, however, be a risky strategy when elements such as Sn, As, Cu, Pb, and Sb occur in the scrap because they have been shown to weaken grain boundaries substantially, leading to embrittlement. Investigation of the element partitioning behavior of scrap-related impurities between phases and lattice defects is needed.

- The downstream production processes (secondary metallurgy, casting, reheating, rolling, recrystallization, etc.) that follow melting must consider the influence of impurity elements on the properties and behavior of steels during processing.
- To deal with the effects of tramp elements, solidification, solutionizing, and heat treatment can be adjusted.
- A link must be made between metallurgical slag and the cement industry, leaving minimal waste that requires disposal.

DISCLOSURE STATEMENT

The authors are not aware of any affiliations, memberships, funding, or financial holdings that might be perceived as affecting the objectivity of this review.

ACKNOWLEDGMENTS

I.S.F. acknowledges financial support through CAPES (Coordenação de Aperfeiçoamento de Pessoal de Nível Superior) and the Alexander von Humboldt Foundation (grant 88881.512949/2020–01). H.S. acknowledges financial support through the Heisenberg Program of the Deutsche Forschungsgemeinschaft (grant SP1666/1–2). Funding by the European Union is acknowledged, through the project ROC, sponsored by the European Research Council (ERC) through the ERC advanced grant 101054368.

LITERATURE CITED

1. Raabe D, Tasan CC, Olivetti EA. 2019. Strategies for improving the sustainability of structural metals. *Nature* 575(7781):64–74
2. World Steel Assoc. 2023. 2023 World steel in figures. *World Steel Association*. **https://worldsteel.org/steel-topics/statistics/world-steel-in-figures-2023/**
3. Raabe D. 2023. The materials science behind sustainable metals and alloys. *Chem. Rev.* 123(5):2436–608
4. Allwood JM, Cullen JM, Milford RL. 2010. Options for achieving a 50% cut in industrial carbon emissions by 2050. *Environ. Sci. Technol.* 44(6):1888–94
5. Allwood JM, Cullen JM, McBrien M, Milford RL, Carruth MA, et al. 2011. *Sustainable Materials: With Both Eyes Open*. Cambridge, UK: UIT Cambridge Ltd.
6. Ma Y, Souza Filho IR, Zhang X, Nandy S, Barriobero-Vila P, et al. 2022. Hydrogen-based direct reduction of iron oxide at 700°C: heterogeneity at pellet and microstructure scales. *Int. J. Miner. Metall. Mater.* 29(10):1901–7
7. Vogl V, Åhman M. 2019. What is green steel? Towards a strategic decision tool for decarbonising EU steel. *Proc. 4th ESTAD* 2019:P532
8. Ma Y, Souza Filho IR, Bai Y, Schenk J, Patisson F, et al. 2022. Hierarchical nature of hydrogen-based direct reduction of iron oxides. *Scr. Mater.* 213:114571
9. Arens M, Worrell E, Eichhammer W, Hasanbeigi A, Zhang Q. 2017. Pathways to a low-carbon iron and steel industry in the medium-term – the case of Germany. *J. Clean. Prod.* 163:84–98
10. Cavaliere P. 2022. Flash ironmaking. In *Hydrogen Assisted Direct Reduction of Iron Oxides*, pp. 339–57. Cham, Switz.: Springer
11. Ma Y, Bae JW, Kim S-H, Jovičević-Klug M, Li K, et al. 2023. Reducing iron oxide with ammonia: a sustainable path to green steel. *Adv. Sci.* 10:2300111
12. Souza Filho IR, Springer H, Ma Y, Mahajan A, da Silva CC, et al. 2022. Green steel at its crossroads: hybrid hydrogen-based reduction of iron ores. *J. Clean. Prod.* 340:130805
13. Åhman M, Olsson O, Vogl V, Nyqvist B, Maltais A, et al. 2018. *Hydrogen steelmaking for a low-carbon economy*. Work. Pap. 2018-07, Stockh. Environ. Inst., Stockh., Swed.
14. Souza Filho IR, Ma Y, Kulse M, Ponge D, Gault B, et al. 2021. Sustainable steel through hydrogen plasma reduction of iron ore: process, kinetics, microstructure, chemistry. *Acta Mater.* 213:116971

15. Allanore A, Lavelaine H, Valentin G, Birat JP, Lapicque F. 2008. Iron metal production by bulk electrolysis of iron ore particles in aqueous media. *J. Electrochem. Soc.* 155(9):E125
16. Allanore A, Lavelaine H, Valentin G, Birat JP, Delcroix P, Lapicque F. 2010. Observation and modeling of the reduction of hematite particles to metal in alkaline solution by electrolysis. *Electrochim. Acta.* 55(12):4007–13
17. Holappa L. 2020. A general vision for reduction of energy consumption and CO_2 emissions from the steel industry. *Metals* 10(9):1117
18. Lechtenböhmer S, Schneider C, Roche MY, Höller S. 2015. Re-industrialisation and low-carbon economy—can they go together? Results from stakeholder-based scenarios for energy-intensive industries in the German state of North Rhine Westphalia. *Energies* 8(10):11404–29
19. Lan C, Hao Y, Shao J, Zhang S, Liu R, Lyu Q. 2022. Effect of H_2 on blast furnace ironmaking: a review. *Metals* 12(11):1864
20. Weigel M, Fischedick M, Marzinkowski J, Winzer P. 2016. Multicriteria analysis of primary steelmaking technologies. *J. Clean. Prod.* 112:1064–76
21. Leeson D, Mac Dowell N, Shah N, Petit C, Fennell PS. 2017. A techno-economic analysis and systematic review of carbon capture and storage (CCS) applied to the iron and steel, cement, oil refining and pulp and paper industries, as well as other high purity sources. *Int. J. Greenh. Gas Control* 61:71–84
22. Rissman J, Bataille C, Masanet E, Aden N, Morrow WR, et al. 2020. Technologies and policies to decarbonize global industry: review and assessment of mitigation drivers through 2070. *Appl. Energy.* 266:114848
23. Philibert C. 2019. Direct and indirect electrification of industry and beyond. *Oxford Rev. Econ. Policy.* 35(2):197–217
24. Züttel A, Remhof A, Borgschulte A, Friedrichs O. 2010. Hydrogen: the future energy carrier. *Philos. Trans. R. Soc. A* 368:3329–42
25. Hertwich EG, Ali S, Ciacci L, Fishman T, Heeren N, et al. 2019. Material efficiency strategies to reducing greenhouse gas emissions associated with buildings, vehicles, and electronics—a review. *Environ. Res. Lett.* 14(4):043004
26. Fruehan RJ. 2009. Research on sustainable steelmaking. *Metall. Mater. Trans. B* 40(2):123–33
27. de Souza JFT, Pacca SA. 2021. Carbon reduction potential and costs through circular bioeconomy in the Brazilian steel industry. *Resour. Conserv. Recycl.* 169:105517
28. Kuramochi T. 2016. Assessment of midterm CO_2 emissions reduction potential in the iron and steel industry: a case of Japan. *J. Clean. Prod.* 132:81–97
29. Fan Z, Friedmann SJ. 2021. Low-carbon production of iron and steel: technology options, economic assessment, and policy. *Joule* 5(4):829–62
30. Zhao J, Zuo H, Wang Y, Wang J, Xue Q. 2020. Review of green and low-carbon ironmaking technology. *Ironmak. Steelmak.* 47(3):296–306
31. Broadbent C. 2016. Steel's recyclability: demonstrating the benefits of recycling steel to achieve a circular economy. *Int. J. Life Cycle Assess.* 21(11):1658–65
32. Wang P, Ryberg M, Yang Y, Feng K, Kara S, et al. 2021. Efficiency stagnation in global steel production urges joint supply- and demand-side mitigation efforts. *Nat. Commun.* 12(1):2066
33. Graedel TE, Harper EM, Nassar NT, Reck BK. 2015. On the materials basis of modern society. *PNAS* 112(20):6295–300
34. Sandberg E, Lennox B, Undvall P. 2007. Scrap management by statistical evaluation of EAF process data. *Control Eng. Pract.* 15(9):1063–75
35. Çiftçi BB. 2018. The future of global scrap availability. *World Steel Association*. **https://worldsteel.org/media-centre/blog/2018/future-of-global-scrap-availability/**
36. Oda J, Akimoto K, Tomoda T. 2013. Long-term global availability of steel scrap. *Resour. Conserv. Recycl.* 81:81–91
37. Morfeldt J, Nijs W, Silveira S. 2015. The impact of climate targets on future steel production – an analysis based on a global energy system model. *J. Clean. Prod.* 103:469–82
38. World Steel Assoc. 2018. Is it time for China to switch to electric arc furnace steelmaking? *World Steel Association*. **https://worldsteel.org/media-centre/blog/2018/is-it-time-for-china-to-switch-to-eaf-steelmaking/**

39. Boldrini A, Koolen D, Crijns-Graus W, Worrell E, van den Broek M. 2024. Flexibility options in a decarbonising iron and steel industry. *Renew. Sustain. Energy Rev.* 189:113988
40. World Steel Assoc. 2023. *Steel – the permanent material in the circular economy*. Rep., World Steel Assoc., Brussels, Belgium
41. Hu R, Zhang C. 2017. Discussion on energy conservation strategies for steel industry: based on a Chinese firm. *J. Clean. Prod.* 166:66–80
42. Shatokha V. 2016. Environmental sustainability of the iron and steel industry: towards reaching the climate goals. *Eur. J. Sustain. Dev.* 5(4):289–300
43. He K, Wang L. 2017. A review of energy use and energy-efficient technologies for the iron and steel industry. *Renew. Sustain. Energy Rev.* 70:1022–39
44. Milford RL, Pauliuk S, Allwood JM, Müller DB. 2013. The roles of energy and material efficiency in meeting steel industry CO_2 targets. *Environ. Sci. Technol.* 47(7):3455–62
45. Pauliuk S, Milford RL, Müller DB, Allwood JM. 2013. The steel scrap age. *Environ. Sci. Technol.* 47(7):3448–54
46. Pauliuk S, Kondo Y, Nakamura S, Nakajima K. 2017. Regional distribution and losses of end-of-life steel throughout multiple product life cycles—insights from the global multiregional MaTrace model. *Resour. Conserv. Recycl.* 116:84–93
47. Panasiuk D, Daigo I, Hoshino T, Hayashi H, Yamasue E, et al. 2022. International comparison of impurities mixing and accumulation in steel scrap. *J. Ind. Ecol.* 26(3):1040–50
48. Raabe D, Ponge D, Uggowitzer PJ, Roscher M, Paolantonio M, et al. 2022. Making sustainable aluminum by recycling scrap: the science of "dirty" alloys. *Prog. Mater. Sci.* 128:100947
49. Daigo I, Tajima K, Hayashi H, Panasiuk D, Takeyama K, et al. 2021. Potential influences of impurities on properties of recycled carbon steel. *ISIJ Int.* 61(1):498–505
50. Spooner S, Davis C, Li Z. 2020. Modelling the cumulative effect of scrap usage within a circular UK steel industry-residual element aggregation. *Ironmak. Steelmak.* 47(10):1100–13
51. Hisashige S, Nakagaki T, Yamamoto T. 2019. CO_2 emission reduction and exergy analysis of SMART steelmaking system adaptive for flexible operating conditions. *ISIJ Int.* 59(4):598–606
52. Zhang X, Ma G, Liu M, Li Z. 2019. Removal of residual element tin in the ferrous metallurgy process: a review. *Metals* 9(8):834
53. Daehn KE, Serrenho AC, Allwood J. 2019. Finding the most efficient way to remove residual copper from steel scrap. *Metall. Mater. Trans. B* 50(3):1225–40
54. Bell S, Davis BR, Javaid A, Essadiqi E. 2006. *Effects of impurities in steel*. Rep. 2005-41(CF), Nat. Resour. Can., Hamilton, ON
55. Daigo I, Fujimura L, Hayashi H, Yamasue E, Ohta S, et al. 2017. Quantifying the total amounts of tramp elements associated with carbon steel production in Japan. *ISIJ Int.* 57(2):388–93
56. Gao Z, Sridhar S, Spiller DE, Taylor PR. 2021. Review of impurity removal methods in steel scrap recycling. *J. Solid Waste Technol. Manag.* 47(4):732–45
57. Toi A, Sato J, Kanero T. 1997. Analysis of tramp element in iron scraps. *Tetsu-To-Hagane* 83(12):850–55
58. Igarashi Y, Daigo I, Matsuno Y, Adachi Y. 2007. Estimation of the change in quality of domestic steel production affected by steel scrap exports. *ISIJ Int.* 47(5):753–57
59. Dworak S, Rechberger H, Fellner J. 2022. How will tramp elements affect future steel recycling in Europe? – A dynamic material flow model for steel in the EU-28 for the period 1910 to 2050. *Resour. Conserv. Recycl.* 179:106072
60. Geerlings H, Promel L, Seetharaman S, Clarke A, Klemm-Toole J, Clarke K. 2022. *Maximizing scrap recycling by designing Cu tolerant steel compositions*. Rep., Colo. Sch. Mines, Golden, CO
61. Dubreuil A, Young SB, Atherton J, Gloria TP. 2010. Metals recycling maps and allocation procedures in life cycle assessment. *Int. J. Life Cycle Assess.* 15(6):621–34
62. Ohno H, Matsubae K, Nakajima K, Kondo Y, Nakamura S, Nagasaka T. 2015. Toward the efficient recycling of alloying elements from end of life vehicle steel scrap. *Resour. Conserv. Recycl.* 100:11–20
63. Watari T, Hata S, Nakajima K, Nansai K. 2023. Limited quantity and quality of steel supply in a zero-emission future. *Nat. Sustain.* 6:336–343

64. Raabe D, Sun B, Kwiatkowski Da Silva A, Gault B, Yen HW, et al. 2020. Current challenges and opportunities in microstructure-related properties of advanced high-strength steels. *Metall. Mater. Trans. A* 51(11):5517–86
65. Yen HW, Ooi SW, Eizadjou M, Breen A, Huang CY, et al. 2015. Role of stress-assisted martensite in the design of strong ultrafine-grained duplex steels. *Acta Mater*. 82:100–14
66. Tasan CC, Diehl M, Yan D, Bechtold M, Roters F, et al. 2015. An overview of dual-phase steels: advances in microstructure-oriented processing and micromechanically guided design. *Annu. Rev. Mater. Res.* 45:391–431
67. Bhadeshia HKDH. 2016. Prevention of hydrogen embrittlement in steels. *ISIJ Int*. 56(1):24–36
68. Djukic MB, Bakic GM, Sijacki Zeravcic V, Sedmak A, Rajicic B. 2019. The synergistic action and interplay of hydrogen embrittlement mechanisms in steels and iron: localized plasticity and decohesion. *Eng. Fract. Mech.* 216:106528
69. Bajaj P, Hariharan A, Kini A, Kürnsteiner P, Raabe D, Jägle EA. 2020. Steels in additive manufacturing: a review of their microstructure and properties. *Mater. Sci. Eng. A* 772:138633
70. Song R, Ponge D, Raabe D, Speer JG, Matlock DK. 2006. Overview of processing, microstructure and mechanical properties of ultrafine grained bcc steels. *Mater. Sci. Eng. A* 441(1–2):1–17
71. De Moor E, Gibbs PJ, Speer JG, Matlock D, Schroth JG. Strategies for third-generation advanced high-strength steel development. *Iron Steel Technol.* 7(11):133–44
72. Koyama M, Akiyama E, Lee YK, Raabe D, Tsuzaki K. 2017. Overview of hydrogen embrittlement in high-Mn steels. *Int. J. Hydrog. Energy* 42(17):12706–23
73. Werheit P, Fricke-Begemann C, Gesing M, Noll R. 2011. Fast single piece identification with a 3D scanning LIBS for aluminium cast and wrought alloys recycling. *J. Anal. At. Spectrom.* 26(11):2166–74
74. Rombach G, Bauerschlag N. 2019. LIBS based sorting—a solution for automotive scrap. In *Light Metals 2019*, ed. C Chesonis, pp. 1351–57. Cham, Switz.; Springer
75. Grand View Res. 2023. *Sheet metal market size, share & trends analysis report by material (steel, aluminum), by end-use (automotive & transportation, building & construction), by region, and segment forecasts, 2020–2025*. Rep. GVR-3-68038-775-9, Grand View Res., San Francisco, CA. **https://www.grandviewresearch.com/industry-analysis/sheet-metal-market**
76. WorldAutoSteel. 2023. WorldAutoSteel report on recycling. *WorldAutoSteel*. **https://www.worldautosteel.org/life-cycle-thinking/recycling/**
77. Kuziak R, Kawalla R, Waengler S. 2008. Advanced high strength steels for automotive industry: a review. *Arch. Civ. Mech. Eng.* 8(2):103–17
78. Galán J, Samek L, Verleysen P, Verbeken K, Houbaert Y. 2012. Advanced high strength steels for automotive industry. *Rev. Metal.* 48(2):118–31
79. Bleck W, Guo X, Ma Y. 2017. The TRIP Effect and its application in cold formable sheet steels. *Steel Res. Int.* 88(10):1700218
80. Uthaisangsuk V, Prahl U, Bleck W. 2009. Characterisation of formability behaviour of multiphase steels by micromechanical modelling. *Int. J. Fract.* 157(1–2):55–69
81. Tasan CC, Diehl M, Yan D, Zambaldi C, Shanthraj P, et al. 2014. Integrated experimental-simulation analysis of stress and strain partitioning in multiphase alloys. *Acta Mater*. 81:386–400
82. Seo EJ, Cho L, Estrin Y, De Cooman BC. 2016. Microstructure-mechanical properties relationships for quenching and partitioning (Q&P) processed steel. *Acta Mater*. 113:124–39
83. Birat JP. 2020. Society, materials, and the environment: the case of steel. *Metals* 10(3):331
84. Compañero RJ, Feldmann A, Tilliander A. 2021. Circular steel: how information and actor incentives impact the recyclability of scrap. *J. Sustain. Metall.* 7(4):1654–70
85. Daehn KE, Cabrera Serrenho A, Allwood JM. 2017. How will copper contamination constrain future global steel recycling? *Environ. Sci. Technol.* 51(11):6599–606
86. Graedel TE, Allwood J, Birat JP, Buchert M, Hagelüken C, et al. 2011. What do we know about metal recycling rates? *J. Ind. Ecol.* 15(3):355–66
87. Reck BK, Graedel TE. 2012. Challenges in metal recycling. *Science* 337(6095):690–95
88. Tisza M, Czinege I. 2018. Comparative study of the application of steels and aluminium in lightweight production of automotive parts. *Int. J. Lightweight Mater. Manuf.* 1(4):229–38

89. Richter JL. 2022. A circular economy approach is needed for electric vehicles. *Nat. Electron.* 5(1):5–7
90. Hagelüken C, Goldmann D. 2022. Recycling and circular economy—towards a closed loop for metals in emerging clean technologies. *Miner. Econ.* 35(3–4):539–62
91. Ortego A, Valero A, Valero A, Iglesias M. 2018. Downcycling in automobile recycling process: a thermodynamic assessment. *Resour. Conserv. Recycl.* 136:24–32
92. Valero A, Valero A, Calvo G, Ortego A. 2018. Material bottlenecks in the future development of green technologies. *Renew. Sustain. Energy Rev.* 93:178–200
93. Harvey LDD. 2021. Iron and steel recycling: review, conceptual model, irreducible mining requirements, and energy implications. *Renew. Sustain. Energy Rev.* 138:110553
94. Ohno H, Matsubae K, Nakajima K, Kondo Y, Nakamura S, et al. 2017. Optimal recycling of steel scrap and alloying elements: input-output based linear programming method with its application to end-of-life vehicles in Japan. *Environ. Sci. Technol.* 51(22):13086–94
95. Nakamura S, Kondo Y, Nakajima K, Ohno H, Pauliuk S. 2017. Quantifying recycling and losses of Cr and Ni in steel throughout multiple life cycles using MaTrace-alloy. *Environ. Sci. Technol.* 51(17):9469–76
96. Lu X, Hiraki T, Nakajima K, Takeda O, Matsuabe K, et al. 2012. Thermodynamic analysis of separation of alloying elements in recycling of end-of-life titanium products. *Sep. Purif. Technol.* 89:135–41
97. Judge WD, Paeng J, Azimi G. 2022. Electrorefining for direct decarburization of molten iron. *Nat. Mater.* 21(10):1130–36
98. Cann JL, De Luca A, Dunand DC, Dye D, Miracle DB, et al. 2021. Sustainability through alloy design: challenges and opportunities. *Prog. Mater. Sci.* 117:100722
99. Miller WS, Zhuang L, Bottema J, Wittebrood AJ, De Smet P, et al. 2000. Recent development in aluminium alloys for the automotive industry. *Mater. Sci. Eng. A* 280(1):37–49
100. Stemper L, Tunes MA, Tosone R, Uggowitzer PJ, Pogatscher S. 2021. On the potential of aluminum crossover alloys. *Prog. Mater. Sci.* 124:100873
101. Paraskevas D, Ingarao G, Deng Y, Duflou JR, Pontikes Y, Blanpain B. 2019. Evaluating the material resource efficiency of secondary aluminium production: a Monte Carlo-based decision-support tool. *J. Clean. Prod.* 215:488–96
102. Modaresi R, Müller DB. 2012. The role of automobiles for the future of aluminum recycling. *Environ. Sci. Technol.* 46(16):8587–94
103. Løvik AN, Modaresi R, Müller DB. 2014. Long-term strategies for increased recycling of automotive aluminum and its alloying elements. *Environ. Sci. Technol.* 48(8):4257–65
104. Duan J, Farrugia D, Davis C, Li Z. 2022. Effect of impurities on the microstructure and mechanical properties of a low carbon steel. *Ironmak. Steelmak.* 49(2):140–46
105. Ahmed S, Sabr A, Peltola A, Oja O, Järn S, et al. 2023. The effect of scrap originating trace elements on the properties of low alloyed steels. *IOP Conf. Ser. Mater. Sci. Eng.* 1284(1):012041
106. Kato K, Ono H. 2021. Effect of ratio of scrap to iron source on slag-metal reaction at the bottom of blast furnace and packed bed type partial smelting reduction furnace. *ISIJ Int.* 61(12):2979–90
107. Lu C, Wang W, Zeng J, Zhu C. 2024. Sub-rapid solidified high copper-bearing steel with excellent resistance to hot shortness. *Scr. Mater.* 239:115800
108. Savov L, Janke D. 1998. Recycling of scrap in steelmaking in view of the tramp element problem. *METALL* 52(6):374–83
109. Gramlich A, Hinrichs T, Springer H, Krupp U. 2023. Recycling-induced copper contamination of a 42CrMo4 quench and tempering steel: alterations in transformation behavior and mechanical properties. *Steel Res. Int.* 94(3):2200623
110. Ono H, Maeda T, Konishi H. 2018. Interaction coefficients of B, Co and Ni on Cu in molten iron. *Tetsu-To-Hagane* 104(3):121–27
111. Kondo Y. 2004. Behaviour of copper during high temperature oxidation of steel containing copper. *ISIJ Int.* 44(9):1576–80
112. Liu Z, Lin Z, Qiu Y, Li N, Liu X, Wang G. 2007. Segregation in twin roll strip cast steels and the effect on mechanical properties. *ISIJ Int.* 47(2):254–58
113. Gudenau HW, Kleinschmidt G. 1996. Removal of impurities from scrap and dust. *ISIJ Int.* 36(Suppl.):S235–38

114. Shibata K, Seo SJ, Kaga M, Uchino H, Sasanuma A, et al. 2002. Suppression of surface hot shortness due to Cu in recycled steels. *Mater. Trans.* 43(3):292–300
115. Hammer B, Kawalla R, Reip CP. 2001. Influence of residuals on the metallurgical features of low carbon steel grades. *Steel Res.* 72(4):146–52
116. Savov L, Volkova E, Janke D. 2003. Copper and tin in steel scrap recycling. *Mater. Geoenviron.* 50(3):627–40
117. Kamguo Kamga H. 2010. *Influence of alloying elements iron and silicon on mechanical properties of aluminum-copper type B206 alloys*. PhD Diss., Univ. Québec, Chicoutimi, Qué.
118. Kunishige K, Hatano M. 2007. Surface hot-shortness of steels induced by a small amount of copper and tin from scrap steels and its suppression methods. *Mater. Sci. Forum.* 539–43:4113–18
119. Andersson JO, Helander T, Höglund L, Shi P, Sundman B. 2002. Thermo-Calc & DICTRA, computational tools for materials science. *Calphad* 26(2):273–312
120. Thermo-Calc Softw. 2023. Steel and Fe-alloys databases. *Thermo-Calc Software.* **https://thermocalc.com/products/databases/steel-and-fe-alloys/**
121. Thermo-Calc Softw. 2023. Metal slag and oxides database. *Thermo-Calc Software.* **https://thermocalc.com/products/databases/metal-oxide-solutions/**
122. IUPAC. 2006. Activity. *Compendium of Chemical Terminology*, 3rd ed. **https://goldbook.iupac.org/terms/view/A00115**
123. Kondo Y, Tanei H. 2015. Effect of oxygen concentration on surface hot shortness of steel induced by copper. *ISIJ Int.* 55(5):1044–47
124. Sahoo G, Deepa M, Singh B, Saxena A. 2016. Hot ductility and hot-shortness of steel and measurement techniques: a review mechanism of hot shortness. *J. Met. Mater. Miner.* 26(2). **https://www.doi.org/10.14456/jmmm.2016.5**
125. IUPAC. 2006. Evaporation. *Compendium of Chemical Terminology*, 3rd ed. **https://goldbook.iupac.org/terms/view/E02227**
126. Peter J, Peaslee KD, Robertson DGC, Thomas BG. 2005. Experimental study of kinetic processes during the steel treatment at two LMF's. In *AISTech 2005 & ICS: Conference Proceedings*, pp. 959–67. Warrendale, PA: Assoc. Iron Steel Technol.
127. Harada A, Maruoka N, Shibata H, Kitamura SY. 2013. A kinetic model to predict the compositions of metal, slag and inclusions during ladle refining: part 1. Basic concept and application. *ISIJ Int.* 53(12):2110–17
128. Van Ende MA, Jung IH. 2017. A kinetic ladle furnace process simulation model: effective equilibrium reaction zone model using FactSage macro processing. *Metall. Mater. Trans. B* 48(1):28–36
129. Van Ende MA, Jung I. 2015. A kinetic process simulation model for basic oxygen furnace (BOF): importance of slag chemistry for BOF operation. *CAMP-ISIJ* 28:527–30
130. Van Ende MA. 2022. Development of an electric arc furnace simulation model using the effective equilibrium reaction zone (EERZ) approach. *JOM* 74:1610–23
131. Graham KJ, Irons GA. 2009. Toward integrated ladle metallurgy control. *Iron Steel Technol.* 6(1):164–73
131a. Preßlinger H. 1997. Verhalten der Begleit- und Spurenelemente bei der LD-Stahlerzeugung und deren Auswirkungen auf die Stahleigenschaften. In *Kontaktstudium Metallurgie*, Teil IV, *Recycling*. Freiberg, Ger.: Ver. Dtsch. Eisenhüttenleute
132. Daehn K, Basuhi R, Gregory J, Berlinger M, Somjit V, Olivetti EA. 2022. Innovations to decarbonize materials industries. *Nat. Rev. Mater.* 7:275–94
133. Serrano L, Lewandrowski T, Liu P, Kaewunruen S. 2017. Environmental risks and uncertainty with respect to the utilization of recycled rolling stocks. *Environments* 4(3):62
134. Zhu Y, Chappuis LB, De Kleine R, Kim HC, Wallington TJ, et al. 2021. The coming wave of aluminum sheet scrap from vehicle recycling in the United States. *Resour. Conserv. Recycl.* 164:105208
135. Hatayama H, Daigo I, Matsuno Y, Adachi Y. 2010. Outlook of the world steel cycle based on the stock and flow dynamics. *Environ. Sci. Technol.* 44(16):6457–63
136. Dworak S, Fellner J. 2021. Steel scrap generation in the EU-28 since 1946 – sources and composition. *Resour. Conserv. Recycl.* 173:105692
137. Ono K, Ichise E, Suzuki RO, Hidani T. 1995. Elimination of copper from the molten steel by NH_3 blowing under reduced pressure. *Steel Res.* 66(9):372–76

138. Sasabe M, Harada E, Yamashita S. 1996. Removal of copper from carbon saturated molten iron by using $FeCl_2$. *Tetsu-To-Hagane* 82(2):129–34
139. Eliasson J, Siwecki T, Hutchinson B. 2006. Processing of copper-containing steel via strip casting—a laboratory evaluation. *Steel Res. Int.* 77(6):409–15
140. Kondo Y. 2006. Behaviour of copper and nickel during high temperature oxidation of steel containing them. *Mater. Sci. Forum.* 522–23:53–60
141. Kondo Y. 2023. Review of oxide scale in hot-rolling process. *Tetsu-To-Hagane* 109(2):87–105
142. Uchino H, Nagasaki C, Kaga M, Seo S-J, Asakura K, Shibata K. 2001. Effects of C and P on surface hot shortness of steel due to Cu mixed from steel scrap. *J. Adv. Sci.* 13(3):260–64
143. Comineli O, Qaban A, Mintz B. 2022. Influence of Cu and Ni on the hot ductility of low C steels with respect to the straightening operation when continuous casting. *Metals* 12(10):1671
144. Mintz B, Qaban A, Kang SE. 2023. The influence of small additions of alloying elements on the hot ductility of AHSS steels: a critical review part 2. *Metals* 13(2):406
145. Ruck A, Monceau D, Grabke HJ. 1996. Effects of tramp elements Cu, P, Pb, Sb and Sn on the kinetics of carburization of case hardening steels. *Steel Res.* 67(6):240–46
146. Sampson E, Sridhar S. 2013. Effect of silicon on hot shortness in Fe-Cu-Ni-Sn-Si alloys during isothermal oxidation in air. *Metall. Mater. Trans. B* 44(5):1124–36
147. Mintz B, Comineli O, Karjalainen LP. 2004. *The influence of Ni on the hot ductility of C-Mn-Al, Cu containing steels as a way of preventing "hot shortness*." Paper presented at the 59th Annual Conference of Associação Brasileira de Metalurgia e Materiais, São Paulo, Brazil, July 19–22
148. Kuzuhara S, Sakuma H, Hayashi H, Daigo I. 2017. Spatial distribution of tramp element contents in recycled steel. *ISIJ Int.* 57(4):758–63
149. Skoufari-Themistou L, Crowther DN, Mintz B. 1999. Strength and impact behaviour of age hardenable copper containing steels. *Mater. Sci. Technol.* 15(9):1069–79
150. Leroy V. 1995. *Mechanical working (rolling mills): effects of tramp elements in flat and long products*. Rep. 16672, Eur. Comm., Brussels, Belg.
151. Kondo Y. 2011. Suppression of surface hot shortness caused by copper during hot rolling. *Mater. Sci. Forum.* 696:183–88
152. Kovács A, Pradeep KG, Herzer G, Raabe D, Dunin-Borkowski RE. 2016. Magnetic microstructure in a stress-annealed $Fe_{73.5}Si_{15.5}B_7Nb_3Cu_1$ soft magnetic alloy observed using off-axis electron holography and Lorentz microscopy. *AIP Adv.* 6(5):56501
153. Pradeep KG, Herzer G, Choi P, Raabe D. 2014. Atom probe tomography study of ultrahigh nanocrystallization rates in FeSiNbBCu soft magnetic amorphous alloys on rapid annealing. *Acta Mater.* 68:295–309
154. Lücke K, Hölscher M. 2008. Rolling and recrystallization textures of BCC steels. *Texture Stress Microstruct.* 14(100):585–96
155. Steiner Petrovič D, Jenko M, Godec M, Vodopivec F, Jeram M, Prešern V. 2007. The influence of copper on the microtexture of Fe-Si-Al alloys for non-oriented electrical sheets. *Metalurgija* 46(2):75–78
156. Gutierrez-Urrutia I, Böttcher A, Lahn L, Raabe D, Gutiérrez-Urrutia I, et al. 2014. Microstructure-magnetic property relations in grain-oriented electrical steels: quantitative analysis of the sharpness of the Goss orientation. *J. Mater. Sci.* 49(1):269–76
157. Liu WC, Man CS, Raabe D, Morris JG. 2005. Effect of hot and cold deformation on the recrystallization texture of continuous cast AA 5052 aluminum alloy. *Scr. Mater.* 53(11):1273–77
158. Osei R, Lekakh S, O'Malley R. 2022. Effect of Cu additions on scale structure and descaling efficiency of low C steel reheated in a combustion gas atmosphere. *Oxid. Met.* 98(3–4):363–83
159. Kondo Y. 2007. Effect of atmospheric conditions on copper behaviour during high temperature oxidation of a steel containing copper. *ISIJ Int.* 47(9):1309–14
160. Yin L, Sampson E, Nakano J, Sridhar S. 2011. The effects of nickel/tin ratio on Cu induced surface hot shortness in Fe. *Oxid. Met.* 76(5–6):367–83
161. Lee CG, Kim SJ, Lee TH, Oh CS. 2004. Effects of tramp elements on formability of low-carbon TRIP-aided multiphase cold-rolled steel sheets. *ISIJ Int.* 44(4):737–43

162. Hosseini Far AR, Mousavi Anijdan SH, Abbasi M. 2019. The effect of Ni and Cu addition on mechanical behavior of thermomechanically controlled processed HSLA X100 steels. In *TMS 2019 148th Annual Meeting & Symposium Supplemental Proceedings*, pp. 579–90. Cham, Switz.: Springer
163. Hosseini Far AR, Anijdan SHM, Abbasi SM. 2019. The effect of increasing Cu and Ni on a significant enhancement of mechanical properties of high strength low alloy, low carbon steels of HSLA-100 type. *Mater. Sci. Eng. A* 746:384–93
164. Pierce DT, Jiménez JA, Bentley J, Raabe D, Wittig JE. 2015. The influence of stacking fault energy on the microstructural and strain-hardening evolution of Fe–Mn–Al–Si steels during tensile deformation. *Acta Mater*. 100:178–90
165. Dmitrieva O, Ponge D, Inden G, Millán J, Choi P, et al. 2011. Chemical gradients across phase boundaries between martensite and austenite in steel studied by atom probe tomography and simulation. *Acta Mater*. 59(1):364–74
166. Rana R, Bleck W, Singh SB, Mohanty ON. 2007. Development of high strength interstitial free steel by copper precipitation hardening. *Mater. Lett.* 61(14–15):2919–22
167. Rana R, Bleck W, Singh SB, Mohanty ON. 2007. Laboratory investigations on copper-alloyed interstitial free steel – part II: effect of colling temperature. *Steel Res. Int.* 78(8):622–30
168. Görzen D, Schwich H, Blinn B, Bleck W, Beck T. 2020. Influence of different precipitation states of Cu on the quasi-static and cyclic deformation behavior of Cu alloyed steels with different carbon contents. *Int. J. Fatigue* 136:105587
169. Görzen D, Schwich H, Blinn B, Song W, Krupp U, et al. 2021. Influence of Cu precipitates and C content on the defect tolerance of steels. *Int. J. Fatigue* 144:106042
170. Schwich H, Görzen D, Blinn B, Beck T, Bleck W. 2020. Characterization of the precipitation behavior and resulting mechanical properties of copper-alloyed ferritic steel. *Mater. Sci. Eng. A* 772:138807
171. Jung JG, Jung M, Lee SM, Shin E, Shin HC, Lee YK. 2013. Cu precipitation kinetics during martensite tempering in a medium C steel. *J. Alloys Compd.* 553:299–307
172. Miglin MT, Hirth JP, Rosenfield AR, Clark WAT. 1986. Microstructure of a quenched and tempered Cu-bearing high-strength low-alloy steel. *Metall. Trans. A* 17(5):791–98
173. Xu Z, Li J, Shen X, Allam T, Richter S, et al. 2021. Tailoring the austenite fraction of a Cu and Ni containing medium-Mn steel via warm rolling. *Metals* 11(12):1888
174. Xu Z, Shen X, Allam T, Song W, Bleck W. 2022. Austenite transformation and deformation behavior of a cold-rolled medium-Mn steel under different annealing temperatures. *Mater. Sci. Eng. A* 829:142115
175. Elbeltagy A, Xu Z, Shen X, Krupp U, Song W. 2023. Yield strength enhancement without ductility loss through controlling the intercritical annealing time in medium-Mn steels. *Adv. Eng. Mater.* 25(15):2300067
176. Hao X, Dong J, Mu X, Wei J, Wang C, Ke W. 2019. Influence of Sn and Mo on corrosion behavior of ferrite-pearlite steel in the simulated bottom plate environment of cargo oil tank. *J. Mater. Sci. Technol.* 35(5):799–811
177. Sun M, Yang X, Du C, Liu Z, Li Y, et al. 2021. Distinct beneficial effect of Sn on the corrosion resistance of Cr-Mo low alloy steel. *J. Mater. Sci. Technol.* 81:175–89
178. Janke D, Savov L, Weddige HJ, Schulz E. 2000. Scrap-based steel production and recycling of steel. *Mater. Technol.* 34(6):387–99
179. Sasaki N, Uchida YI, Miki YJ, Matsuno H. 2016. Fundamental study of Sn removal from hot metal by NH_3 gas blowing. *Tetsu-To-Hagane* 102(1):17–23
180. Grabke HJ. 2008. Surface and grain boundary segregation on and in iron and steels. *ISIJ Int.* 29(7):529–38
181. Grabke HJ. 2000. Surface and interface segregation in the oxidation of metals. *Surf. Interface Anal.* 30(1):112–19
182. Faulkner RG. 1981. Non-equilibrium grain-boundary segregation in austenitic alloys. *J. Mater. Sci.* 16(2):373–83
183. Karlsson L, Nordén H, Odelius H. 1988. Overview no. 63 non-equilibrium grain boundary segregation of boron in austenitic stainless steel—I. Large scale segregation behaviour. *Acta Metall.* 36(1):1–12
184. Kuzmina M, Ponge D, Raabe D. 2015. Grain boundary segregation engineering and austenite reversion turn embrittlement into toughness: example of a 9 wt.% medium Mn steel. *Acta Mater*. 86:182–92

185. Raabe D, Ponge D, Dmitrieva O, Sander B. 2009. Designing ultrahigh strength steels with good ductility by combining transformation induced plasticity and martensite aging. *Adv. Eng. Mater.* 11(7):547–55
186. Seah MP. 1980. Grain boundary segregation. *J. Phys. F* 10(6):1043–64
187. Seah MP. 1980. Adsorption-induced interface decohesion. *Acta Metall.* 28(7):955–62
188. Seah MP. 1975. Interface adsorption, embrittlement and fracture in metallurgy. A review. *Surf. Sci.* 53(1):168–212
189. Hondros ED, Seah MP. 2014. Segregation to interfaces. *Int. Met. Rev.* 22(1):262–301
190. Grabke HJ. 1989. Surface and grain boundary segregation on and in iron and steels. *ISIJ Int.* 29(7):529–38
191. Jenko M, Godec M, Viefhaus H, Grabke HJ. 1999. Antimony, tin and selenium segregation in FeSiC alloys. *Mater. Sci. Forum.* 294–96:747–50
192. Clauberg E, Uebing C, Viefhaus H, Grabke HJ. 2000. Surface segregation of antimony on ferritic single crystals. *Surf. Sci.* 454(1):613–17
193. Mast R, Viefhaus H, Grabke HJ. 1999. Grain boundary segregation of antimony in iron base alloys and its effect on toughness. *Steel Res.* 70(6):239–46
194. Hoile S. 2000. Processing and properties of mild interstitial free steels. *Mater. Sci. Technol.* 16(10):1079–93
195. Raabe D, Lücke K. 1992. Rolling and annealing textures of bcc metals. *Scr. Metall. Mater.* 27(Part 1):597–610
196. Hölscher M, Raabe D, Lücke K. 1991. Rolling and recrystallization textures of bcc steels. *Steel Res.* 62:567–75
197. Jenko M, Vodopivec F, Juergen Grabke H, Viefhaus H, Pracek B, et al. 1994. Orientation dependent surface segregation of antimony on non-oriented electrical steel sheet. *Steel Res.* 65(11):500–4
198. Godec M, Jenko M, Grabke HJ, Mast R. 1999. Sn segregation and its influence on electrical steel texture development. *ISIJ Int.* 39(7):742–46
199. Juntunen P, Karjalainen P, Raabe D, Bolle G, Kopio T. 2001. Optimizing continuous annealing of interstitial-free steels for improving deep drawability. *Metall. Mater. Trans. A* 32(8):1989–95
200. Tee JKS, Fray DJ. 1999. Removing impurities from steel scrap using air and chlorine mixtures. *JOM* 51(8):24–27
201. Talapatra A, Datta J, Bandhyopadhyay NR. 2013. Structure-properties relationship of TRIP-assisted steels by non-destructive testing method. *Chem. Mater. Eng.* 1(1):18–27
202. Kim SJ, Lee CG, Lee TH, Lee S. 2000. Effects of coiling temperature on microstructure and mechanical properties of high-strength hot-rolled steel plates containing Cu, Cr and Ni. *ISIJ Int.* 40(7):692–98
203. Choi JH, Jo MC, Lee H, Zargaran A, Song T, et al. 2019. Cu addition effects on TRIP to TWIP transition and tensile property improvement of ultra-high-strength austenitic high-Mn steels. *Acta Mater.* 166:246–60
204. Martins AR, Rizzo F, Coelho D, Speer JG, Matlock D, et al. 2009. Microstructure and mechanical properties of Ni-added high strength steels subjected to quenching and partitioning (Q&P) heat treatment. *Mater. Sci. Technol. Conf. Exhib.* 3:1564–74
205. Pierce DT, Coughlin DR, Clarke KD, De Moor E, Poplawsky J, et al. 2018. Microstructural evolution during quenching and partitioning of 0.2C-1.5Mn-1.3Si steels with Cr or Ni additions. *Acta Mater.* 151:454–69
206. Entezari E, Mousalou H, Yazdani S, González-Velázquez JL, Szpunar JA. 2021. The evaluation of quenching temperature effect on microstructural and mechanical properties of advanced high strength low carbon steel after quenching partitioning treatment. *Procedia Struct. Integr.* 37(C):145–52
207. Mohrbacher H, Kern A. 2023. Nickel alloying in carbon steel: fundamentals and applications. *Alloys* 2(1):1–28
208. Wang MM, Tasan CC, Ponge D, Raabe D. 2016. Spectral TRIP enables ductile 1.1 GPa martensite. *Acta Mater.* 111:262–72
209. Sun B, Kwiatkowski A, Wu Y, Ma Y, Chen H, et al. 2022. Physical metallurgy of medium-Mn advanced high-strength steels. *Int. Mater. Rev.* 68:786–824
210. Li Y, Yuan G, Li L, Kang J, Yan F, et al. 2023. Ductile 2-GPa steels with hierarchical substructure. *Science* 379(6628):168–73

211. Sun B, Palanisamy D, Ponge D, Gault B, Fazeli F, et al. 2019. Revealing fracture mechanisms of medium manganese steels with and without delta-ferrite. *Acta Mater*. 164:683–96
212. Ma Y. 2017. Medium-manganese steels processed by austenite-reverted-transformation annealing for automotive applications. *Mater. Sci. Technol.* 33(15):1713–27
213. Brüx U, Frommeyer G, Grässel O, Meyer LW, Weise A. 2002. Development and characterization of high strength impact resistant Fe-Mn-(Al-, Si) TRIP/TWIP steels. *Steel Res*. 73(6–7):294–98
214. Gramlich A, Stieben A, Menzel M, Pape F, Lüneburg B, Bleck W. 2019. Manganese alloyed Q & T steel with high hardenability for forging parts with large diameters. *J. Heat Treat. Mater.* 74(6):357–65
215. Gramlich A, Schmiedl T, Schönborn S, Melz T, Bleck W. 2020. Development of air-hardening martensitic forging steels. *Mater. Sci. Eng. A* 784:139321
216. Sun B, Lu W, Gault B, Ding R, Makineni SK, et al. 2021. Chemical heterogeneity enhances hydrogen resistance in high-strength steels. *Nat. Mater.* 20:1629–34
217. Ding R, Yao Y, Sun B, Liu G, He J, et al. 2020. Chemical boundary engineering: a new route toward lean, ultrastrong yet ductile steels. *Sci. Adv.* 6(13):eaay1430
218. Kwiatkowski da Silva A, Leyson G, Kuzmina M, Ponge D, Herbig M, et al. 2017. Confined chemical and structural states at dislocations in Fe-9wt%Mn steels: a correlative TEM-atom probe study combined with multiscale modelling. *Acta Mater*. 124:305–15
219. De Cooman BC. 2016. High Mn TWIP steel and medium Mn steel. In *Automotive Steels: Design, Metallurgy, Processing and Applications*, ed. R Rana, SB Singh, pp. 317–85. Duxford, UK: Woodhead Publ.
220. Haupt M, Dutta A, Ponge D, Sandlöbes S, Nellessen M, Hirt G. 2017. Influence of intercritical annealing on microstructure and mechanical properties of a medium manganese steel. *Procedia Eng*. 207:1803–8
221. Itman A, Cardoso KR, Kestenbach HJ. 1997. Quantitative study of carbonitride precipitation in niobium and titanium microalloyed hot strip steel. *Mater. Sci. Technol.* 13(1):49–55
222. Barani AA, Li F, Romano P, Ponge D, Raabe D. 2007. Design of high-strength steels by microalloying and thermomechanical treatment. *Mater. Sci. Eng. A* 463(1–2):138–46
223. Courtois E, Epicier T, Scott C. 2006. EELS study of niobium carbo-nitride nano-precipitates in ferrite. *Micron* 37(5):492–502
224. Cameron BC, Tasan CC. 2019. Microstructural damage sensitivity prediction using spatial statistics. *Sci. Rep.* 9(1):2774
225. De Cooman BC. 2004. Structure–properties relationship in TRIP steels containing carbide-free bainite. *Curr. Opin. Solid State Mater. Sci.* 8(3–4):285–303
226. Nazari KA, Shabestari SG. 2009. Effect of micro alloying elements on the interfacial reactions between molten aluminum alloy and tool steel. *J. Alloys Compd.* 478(1–2):523–30
227. Hunkel M. 2021. Segregations in steels during heat treatment—a consideration along the process chain. *J. Heat Treat. Mater.* 76(2):79–104
228. Grabke HJ, Möller R, Erhart H, Brenner SS. 1987. Effects of the alloying elements Ti, Nb, Mo and V on the grain boundary segregation of P in iron and steels. *Surf. Interface Anal.* 10(4):202–9
229. Miranda AM, Assis PS, Brooks GA, Rhamdhani MA, Fontana A, et al. 2019. Monitoring of less-common residual elements in scrap feeds for EAF steelmaking. *Ironmak. Steelmak.* 46(7):598–608
230. Yamada Y, Kuwabara T. 2007. *Materials for Springs*. Berlin: Springer
231. Li F, Barani AA, Ponge D, Raabe D. 2006. Austenite grain coarsening behaviour in a medium carbon Si-Cr spring steel with and without vanadium. *Steel Res. Int.* 77(8):590–94
232. Hayakawa Y. 2020. Recent developments in non-oriented electrical steels. *Tetsu-To-Hagane* 106(10):683–96
233. Kawalla R, Stöcker A, Prahl U, Wei X, Dierdorf J, et al. 2018. Low-loss FeSi sheet for energy-efficient electrical drives. *AIMS Mater. Sci.* 5(6):1184–98
234. Benzing JT, Bentley J, McBride JR, Ponge D, Han J, et al. 2017. Characterization of partitioning in a medium-Mn third-generation AHSS. *Microsc. Microanal.* 23(S1):402–3
235. Archie F, Li X, Zaefferer S. 2017. Micro-damage initiation in ferrite-martensite DP microstructures: a statistical characterization of crystallographic and chemical parameters. *Mater. Sci. Eng. A* 701:302–13
236. Hoefnagels JPM, Tasan CC, Maresca F, Peters FJ, Kouznetsova VG. 2015. Retardation of plastic instability via damage-enabled microstrain delocalization. *J. Mater. Sci.* 50(21):6882–97

237. Matlock DK, Speer JG. 2009. Third generation of AHSS: microstructure design concepts. In *Microstructure and Texture in Steels*, ed. A Haldar, S Suwas, D Bhattacharjee, pp. 185–205. London: Springer
238. Calcagnotto M, Ponge D, Raabe D. 2008. Ultrafine grained ferrite/martensite dual phase steel fabricated by large strain warm deformation and subsequent intercritical annealing. *ISIJ Int*. 48(8):1096–101
239. Yan D, Tasan CC, Raabe D. 2015. High resolution in situ mapping of microstrain and microstructure evolution reveals damage resistance criteria in dual phase steels. *Acta Mater*. 96:399–409
240. Teo PT, Zakaria SK, Salleh SZ, Taib MAA, Sharif NM, et al. 2020. Assessment of electric arc furnace (EAF) steel slag waste's recycling options into value added green products: a review. *Metals* 10(10):1347
241. Roters F, Eisenlohr P, Hantcherli L, Tjahjanto DD, Bieler TR, Raabe D. 2010. Overview of constitutive laws, kinematics, homogenization and multiscale methods in crystal plasticity finite-element modeling: theory, experiments, applications. *Acta Mater*. 58(4):1152–211
242. Deleted in proof
243. Graham MJ, Wild RK, Grabke HJ. 1994. Interfacial chemistry of high temperature scaling. *Mater. High Temp*. 12(2–3):135–39
244. Paju M, Viefhaus H, Grabke HJ. 1988. Phosphorus segregation in austenite in Fe–P–C, Fe–P–B and Fe–P–C–B alloys. *Steel Res*. 59(8):336–43
245. Ruedl E, Sasaki T. 1983. Effect of lithium on grain-boundary precipitation in a Cr-Mn austfnitic steel. *J. Nucl. Mater.* 116(1):112–22
246. Barnett MR, Senadeera M, Fabijanic D, Shamlaye KF, Joseph J, et al. 2020. A scrap-tolerant alloying concept based on high entropy alloys. *Acta Mater*. 200:735–44
247. Pérez I, Arribas M, Aranguren I, Mangas Á, Rana R, et al. 2019. Processing of new dual-phase (DP) and complex-phase (CP) steels for automotive applications by tailored hot forming routes. *AIP Conf. Proc.* 2113:170008
248. Krauss G. 2001. Deformation and fracture in martensitic carbon steels tempered at low temperatures. *Metall. Mater. Trans. A* 32(4):861–77
249. Calcagnotto M, Ponge D, Raabe D. 2010. Effect of grain refinement to 1μm on strength and toughness of dual-phase steels. *Mater. Sci. Eng. A* 527(29–30):7832–40
250. Han J, Kwiatkowski Da Silva A, Ponge D, Raabe D, Lee SM, et al. 2017. The effects of prior austenite grain boundaries and microstructural morphology on the impact toughness of intercritically annealed medium Mn steel. *Acta Mater*. 122:199–206
251. Calcagnotto M, Ponge D, Demir E, Raabe D. 2010. Orientation gradients and geometrically necessary dislocations in ultrafine grained dual-phase steels studied by 2D and 3D EBSD. *Mater. Sci. Eng. A* 527(10–11):2738–46
252. Song R, Ponge D, Raabe D. 2005. Influence of Mn content on the microstructure and mechanical properties of ultrafine grained C–Mn steels. *ISIJ Int*. 45(11):1721–26
253. Schemmann L, Zaefferer S, Raabe D, Friedel F, Mattissen D. 2015. Alloying effects on microstructure formation of dual phase steels. *Acta Mater*. 95:386–98
254. Nakajima K, Takeda O, Miki T, Matsubae K, Nagasaka T. 2011. Thermodynamic analysis for the controllability of elements in the recycling process of metals. *Environ. Sci. Technol.* 45(11):4929–36